

# Circuit Mechanisms for Spatial Relation Generation in Diffusion Transformers

Binxu Wang\*  
 Kempner Institute, Harvard University  
 binxu.wang@hms.harvard.edu

Jingxuan Fan\*  
 Harvard University  
 jfan@g.harvard.edu

Xu Pan\*  
 Harvard University  
 xupan@fas.harvard.edu

## Abstract

*Diffusion Transformers (DiTs) have greatly advanced text-to-image generation, but models still struggle to generate the correct spatial relations between objects as specified in the text prompt. In this study, we adopt a mechanistic interpretability approach to investigate how a DiT can generate correct spatial relations between objects. We train, from scratch, DiTs of different sizes with different text encoders to learn to generate images containing two objects whose attributes and spatial relations are specified in the text prompt. We find that, although all the models can learn this task to near-perfect accuracy, the underlying mechanisms differ drastically depending on the choice of text encoder. When using random text embeddings, we find that the spatial-relation information is passed to image tokens through a two-stage circuit, involving two cross-attention heads that separately read the spatial relation and single-object attributes in the text prompt. When using a pretrained text encoder (T5), we find that the DiT uses a different circuit that leverages information fusion in the text tokens, reading spatial-relation and single-object information together from a single text token. We further show that, although the in-domain performance is similar for the two settings, their robustness to out-of-domain perturbations differs, potentially suggesting the difficulty of generating correct relations in real-world scenarios.*

## 1. Introduction

Diffusion and flow model [1, 7, 13, 20, 29] has been leading the charge in generative modeling across many domains, including image, video, and shape[14], etc. Specifically, conditional diffusion transformers (DiT) for text-to-image generation (T2I) have unleashed enormous creativity in both industry and the research community, enabling high-fidelity, diverse image synthesis from natural language prompts [28]. However, many current T2I models often fail to follow prompts when composing multiple objects

onto a scene [6], particularly in arranging their spatial relations [9, 15, 16]. While the field is fast advancing in generating accurate attributes for single objects, the improvement of generating correct relations between objects is comparatively slow (Fig. 10). Increasing attention has been drawn to this problem, and multiple remedies have been proposed recently, including layout conditioning, cross attention guidance, curriculum learning and finetuning with domain-specific data ([3, 4, 10, 19]). However, few work has approached this problem by understanding the underlying circuit for correct composition of multiple objects. Inspired by an emerging research field, named “mechanistic interpretability”, that reverse-engineer a model’s internal computations to identify how neurons, attention heads, and weights implement algorithms and produce specific outputs, we study this relation generation problem in a mechanistic fashion, with a goal to understand how T2I models can generate spatial relations under different architectural and hyperparameter configurations, and under what conditions they could fail.

To study this problem in a controlled setting, we construct a text-to-image task and train T2I models from scratch. The task is to generate two objects (with compositional shape and color feature) in the scene with one of eight spatial relations specified in the text. Then we delve into the underlying transformer circuits to achieve this task, and find the actual circuits used to solve this task heavily depend on the choice of text encoders. With random token embedding, the T2I model implements a two-stage circuits with two specialized cross-attention heads for reading relation information and single object information respectively. With T5 text encoder, which produces token embeddings that are semantically mixed, the T2I model indeed reads all the relation and single-object information from a single token. We justify the circuits we found by both ablation and causal manipulation. We further find that though the two circuits mechanism achieves similar task accuracy, their robustness is different upon small perturbation in the text prompt. The accuracy with T5 encoder collapses after perturbing by adding an extra filler token in the prompt.

Our study sheds light on several previously unresolved

\*equal contribution

questions: 1) It was unclear how neural networks encode and use non-commutative relations between objects [31]. Our work reveals a concrete circuit in diffusion transformers that image tokens can read and implement the relational information in the text, offering a mechanistic example that may generalize to other relational reasoning tasks. 2) The iterative nature of sampling has been an obstacle that complicates attention map analysis and circuit finding in diffusion models. We provide a systematic approach to summarize attention maps and pinpoint heads underlying certain communication patterns, which could be adapted as a general tool to study DiT. 3) Previous studies attributed the spatial relation generation failure to particular stages, e.g. cross attention ([4, 25]) or text encoding ([17, 33]). In this study, we offer a holistic view that bridges these threads. In our toy setting, the T5-based DiT relies on the information fusion by T5 for spatial relationships while the RTE-based DiT implements its own circuits for generating relations. This suggests that the embedding model could be the bottleneck for generating spatial relations in real-world scenarios, making embedding model improvements potentially more critical than DiT modifications.

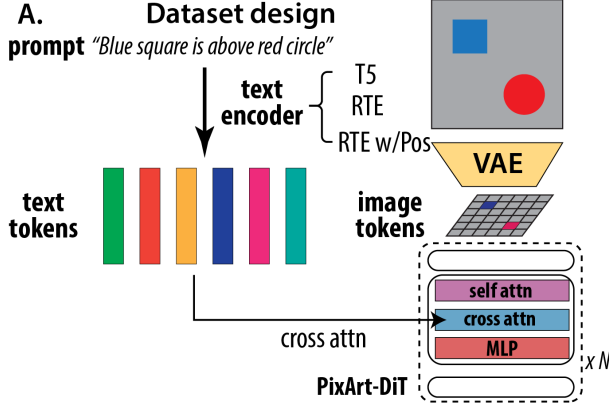


**Figure 1. Schematics of the model and task.** Our T2I model architecture adopted the design of PixArt [5]. There are three main components: the **text encoder** that processes tokenized natural language prompts into text embeddings, the **VAE** that processes image inputs into image tokens, and the **Diffusion Transformer (DiT)** which is the backbone of the denoising diffusion process. The text information routes through the cross attention mechanism in each DiT block and influence the denoising of image tokens. The task is to generate two objects with a specified spatial relation.

## 2. Background

**Spatial generation failure in T2I models** Failure in multi-object spatial relation generation has been widely reported in T2I models. While new models improved significantly in generating accurate single object attributes, the

improvement of generating correct relations between objects is less impressive (Fig.10). One common view is that spatially localized cross-attention grounds object placement. Building on this hypothesis, recent work tackles spatial-relation failures by directly manipulating attention at inference. [4] proposes to specifically enhance the cross-attention to subject tokens to prevent catastrophic neglect and improve attribute binding; [25] optimizes cross- and self-attention using layout-derived losses—via user boxes or LLM-proposed layouts—to enforce multi-object placement and spatial relations. On the other hand, works like [33] and [17] argue that the poor spatial performance of T2I models stems from the limitations of text encoders. [33] finds that text encoders used across frontier T2I models do not sufficiently preserve spatial relations information in their encoding. Similarly, [17] argues that multiple image properties including spatial relations cannot be simultaneously encoded by CLIP. Our work is unique in that we unite these two views: we show that different information encoding from text-encoders contribute to distinctive attention patterns and circuits.

**Interpretability in diffusion** The work that shares the most similar interest with us is [23, 24], which studies the learning dynamics of composition of attributes on a single object in a conditional diffusion model using a minimalist dataset. The key difference is that we focus on the generation of a composition of multiple objects on the scene instead of a single object. Moreover, we study the architecture where the conditioning signal is encoded by multiple word vectors (e.g. T5 encoder) and passed to image tokens via cross attention, instead of a single vector summing all attributes as in [23]. Our setup is more closely related to modern T2I frameworks [5, 27, 32].

## 3. Train T2I models to generate spatial relation

To understand the T2I model’s spatial relationship generation mechanism and failure in a controlled manner, we construct a minimal text-image dataset and train DiT-based T2I models of different sizes and text encoders from scratch. We make sure that both single object features and object relation properties are reliably learned and amenable to mechanistic analysis.

**Dataset setup** We reason that such a dataset should have following properties: 1) multiple objects in the scene with distinct features, 2) objects arranged to satisfy specific spatial relations described by the prompt, and 3) samples are simple enough to be evaluated rigorously. Guided by this principle, we design a dataset of the following format: each sample consists of a prompt in the format [descriptor A] [object A] [relation] [descriptor B] [object B],

e.g., “*red square above and to the left of blue circle*”, and a corresponding image with two objects positioned on a gray background (Fig. 1A). We use three shapes (*circle, triangle, square*), two colors (*red, blue*), and eight spatial relations: *left, right, above, below, upper left, upper right, lower left, lower right*. The shape and color of the two objects are always distinct, and their positions are arranged to avoid collisions. The color descriptors A and B are randomly dropped, and spatial relations are described with multiple paraphrases to add variability (details in App. B.1).

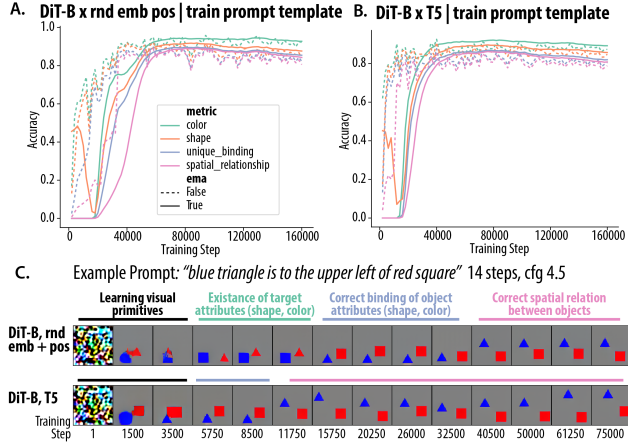


Figure 2. **Training dynamics of the T2I models (DiT-B).** **A)** and **B)** Both models trained with random token embedding and T5 can achieve good accuracy on the task. Solid lines shows the result of model using exponential moving averaged (ema) weights, while dashed line shows the non-averaged weights. **C)** The task is learned in distinct stages. In both models, they first learn to generate objects but with wrong attributes binding, then they the correct binding of single-object attributes (e.g. red square), finally they learn the correct spatial relation. (see App.A.2 for other models).

**Model architecture** We use a DiT-based T2I model, following a PixArt-style architecture representative of the state-of-the-art open-source DiT models [5]. We train several model sizes with patch size 2: DiT-B (12 layers, 12 heads, 768 latent dimensions), mini (6L, 6H, 384-d), micro (6L, 3H, 192-d), and nano (3L, 3H, 192-d). Following common practice, images are encoded with the VAE pretrained from Stable Diffusion [27]. As for text conditioning, we compare three encoders: (i) T5-XXL [26]; (ii) a random token encoder with sinusoidal positional encoding (RTE); (iii) RTE without positional encoding. The RTE maps each token ID to a fixed Gaussian-sampled vector whose dimension and norm match those of T5 embeddings. This comparison tests whether the diffusion transformer can learn object relations without semantic or contextual structure in the text embeddings, enabling us to localize the model’s relational computations (Fig. 1A). (details in App. B.2).

**Sampling and evaluation** Throughout training, we evaluate model generations on 96 prompts spanning 8 spatial relations and 12 object pairs. Generation is performed on multiple random seeds with the default sampler (DPM-Solver++ with 14 steps [22]) and classifier-free guidance of 4.5 [12]. We evaluate the consistency of generated images with the prompts using classic segmentation and classification tools from cv2 [2]. Specifically, we evaluate four aspects of samples: 1) existence of correct colors on the image, denoted as *color*, 2) existence of correct shapes on the image, denoted as *shape* 3) correctness of shape color binding on the two objects, denoted as *unique\_binding* and 4) correctness of spatial relation between the identified two objects, denoted as *spatial\_relation*. Each metric produces a binary (0,1) score for each sample, which we then average to obtain the model’s accuracy.

**Model comparison** Accuracy on all four metrics increases with model parameter sizes up to the DiT-mini configuration; accuracy gains from DiT-mini to DiT-B are marginal (Tab. 2). All trained models at the largest parameter size (DiT-B) show high accuracy in *color* and *shape*, but the *unique\_binding* and *spatial\_relation* accuracy varies significantly depending on the chosen text encoders (Tab. 2). Both RTE and T5 achieve strong *unique\_binding* and *spatial\_relation* accuracy, indicating that **pretrained semantic structure (T5) is not strictly required for learning object relations**. However, RTE without positional encoding is significantly worse on these metrics. Since text enters only through the cross attention mechanism, without positional cues, the DiT output is invariant to permutation of text embeddings. For instance, “*red A on top of blue B*” and “*blue B on top of red A*” collapse to the same bag of words, yielding identical outputs. Adding positional information resolves this ambiguity.

**Training dynamics** Having established the end-point performance trends across models, we next examine how these capabilities emerge during training. For both T5-DiT and RTE-DiT models, we evaluate models with the exponential moving average (EMA) weights [18] following common practice and the accuracy curves averaged across multiple runs are showed. We consistently observe that *color* accuracy converges first, followed by *shape* and then *unique\_binding*. *spatial\_relation* is learned the slowest (Fig. 2A.B.), indicating that relational composition is more challenging to learn than single-object attributes or bindings. Comparing across the two text encoders, we observe that T5-DiT models converge to the final accuracy faster across all four evaluation metrics. Moreover, the temporal gaps between the convergence of different metrics are tighter. We also provide generation examples at different training steps for visual examination (Fig. 2C.). The dif-

ferent learning dynamics provide the first hint that the two family of models potentially use different internal mechanisms to accomplish the same generation task.

## 4. Relation generation circuits in RTE-DiT

### 4.1. Attention synopsis

In DiT-based architecture, cross-attention provides the only mechanism by which text prompts can modulate the image tokens during each denoising step. Therefore, we examine the cross-attention patterns to gain insights into how text on single object feature and spatial relations guide correct generations. Given the large number of DiT’s cross attention maps ( $[ \text{layers} \times \text{heads} \times \text{time steps} \times \text{condition} \text{ vs } \text{uncondition pass} \times \text{number of tokens} ]$ ), it is impractical to perform visual inspection individually. Moreover, simply averaging attention maps over different samples and prompts can obscure specific interactions. Therefore, we develop a scalable paradigm to analyze and quantitatively summarize the cross-attention head patterns, which we term *Attention Synopsis* (Fig. 3) Equipped with this method, we efficiently search through over 10 million attention maps to trace stable text-to-image information flow and localize the relevant circuit mechanisms for spatial relations generation. Specifically, we leverage the fact that token categories are identifiable in both image and text (image tokens by object segmentation, text tokens by semantic attribute). We then aggregate attention within categories, yielding interpretable category-to-category interaction patterns. After this aggregation, we reduce the cross-attention map tensor dimension to  $[ \text{num layer} \times \text{num head} \times \text{num time steps} ]$ . Observing that the attention maps usually change smoothly across time, we further calculate the mean attention maps over time steps, reducing the tensor to shape  $[ \text{num layer}, \text{num head} ]$ , which we denote as the *attention map synopsis*. Each entry denotes the mean *attention transmission energy* between a specific text–image token category pair (details in App. B.5).

Many previous works have reported the cross attention communication between the text token of a single object and the corresponding object in the image [30], and this property is leveraged to control generation [11, 21]. These findings suggest that there is coupling between single object tokens across text and image modality, supporting faithful generation. However, less is known about whether text tokens describing *spatial relations between* objects exhibit similar properties. Therefore, we leverage the *Attention Synopsis* method to examine all category-to-category cross-attention patterns, especially focusing on the spatial relations category. We show results for RTE-DiT in this section and T5-DiT in Section 5.

In RTE-DiT, we find a minimal circuit that enables generation of correct objects at correct spatial locations. The

circuit consists of two key cross attention heads which we discuss in details below.

### 4.2. Spatial relation head

We first use attention synopses to look for cross attention heads that pass information from relational text tokens to image tokens. We find, indeed, there are specialized heads for this transmission. In the case of “object1” (i.e. the first object in the text), there is only one head (L2H8) that dominates, while in the case of “object2”, there are a small number of heads that have this role (Fig. 4A). We also find a similar pattern in models of other sizes (App.A.3). We name these heads “**spatial relation head**”. Examining their attention score towards relation words across sampling steps (Fig. 4B), we find that they activate immediately (at step 0), before any image information is available. Their activation patterns align with the spatial region associated with the relation token and progressively concentrate toward the generated object. These observations imply that the query which maximizes the attention score of this head is potentially aligned with the positional embedding. We verify this hypothesis by checking the QK circuit [8] of L2H8 (Fig. 4C). The head transforms sinusoidal positional embeddings from image tokens into the query space ( $Q$ ) and MLP-transformed relation-word embeddings<sup>1</sup> into the key space ( $K$ ) via learned linear layers ( $W_q, W_k$ ). This  $Q, K$  transformation aligns specific coordinates in the image grid with the semantics of spatial relation tokens. The resulting inner-product maps (Fig. 4C) form smooth gradients whose orientation reflects the spatial relations (e.g., “above” produces a vertical gradient, with highest energy on top). These gradients act as positional tags, marking the regions of the canvas where the first object should be placed. Downstream heads then read these tags to guide accurate object placement and generation. Notably, this mechanism is strikingly similar to the molecular gradients that direct embryonic cells into specific organs, just as tokens “develop” into the proper visual features.

### 4.3. Object Generation Head

The spatial relation head allows differential tagging of image tokens based on relational text tokens. To successfully generate the composite scene, the model also needs to generate the correct object on the tagged canvas. To this purpose, we examine cross attention heads that pass object shape information from text tokens to image tokens. We identify a prominently active head—Layer 4, Head 3 (L4H3) that consistently mediates communication between an object’s image tokens and its corresponding shape word in the prompt (Fig. 5A). This linkage is invariant to both the object’s position in the sentence (Shape 1 or 2) and the

<sup>1</sup>In the PixArt architecture, frozen text embeddings are first passed through a learnable MLP projection before entering the attention layers.

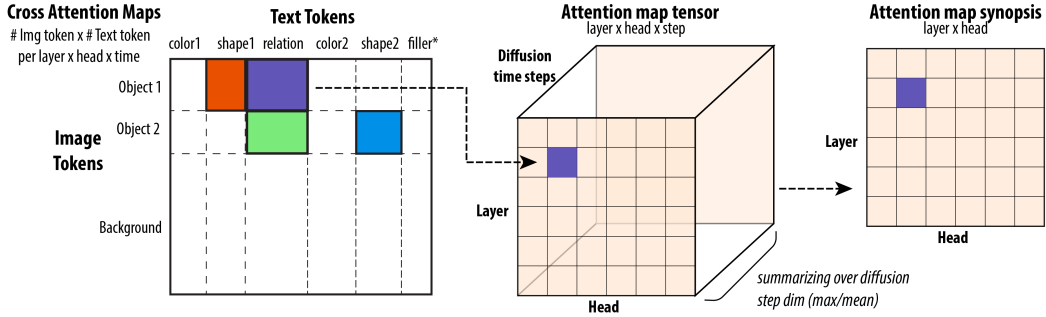


Figure 3. **Illustration of our method to find relevant heads**, which we name as ‘‘attention synopsis’’. The giant attention tensor is first reduced to those only between two interested groups of tokens (e.g. the relation token regardless specific words, or an object token regardless where or what it is). Then the reduced attention tensor is averaged over diffusion time steps, resulting in a layer  $\times$  head map which we use to pinpoint relevant heads.

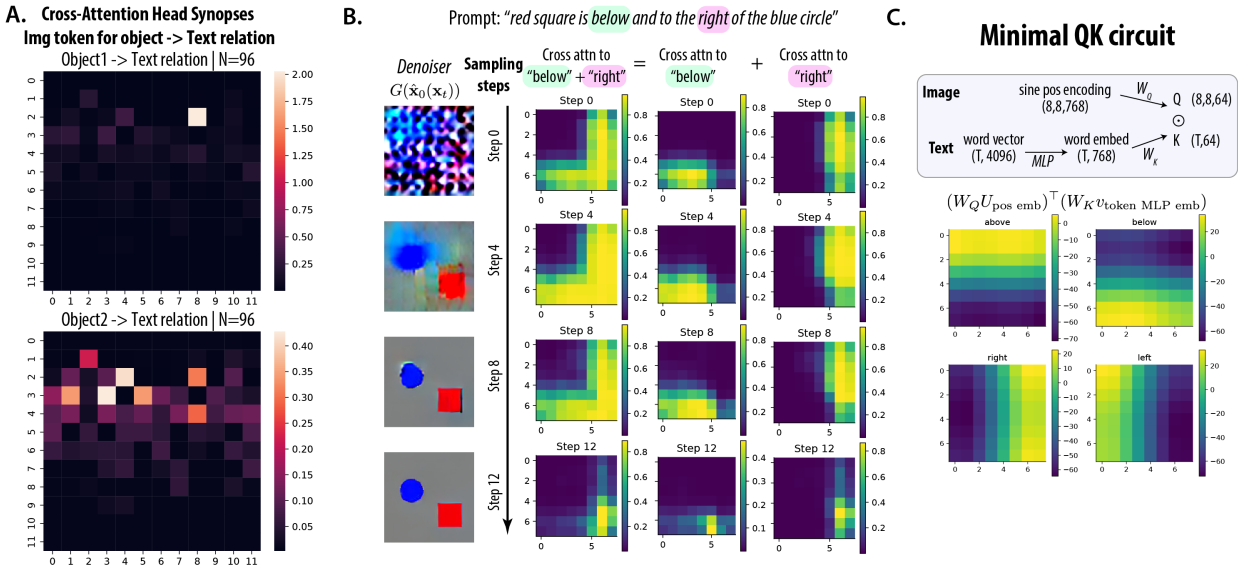


Figure 4. **The spatial relation heads in random-embedding-based T2I.** A) We find specialized cross attention heads that contributes to the object image tokens (top: the object1 in the text; bottom: the object2 in the text) attending to the relation text tokens. B) We show the activation of this head across images tokens and sampling steps. The map for the composite relation ‘‘below and right’’ decomposes cleanly as the sum of the maps for ‘‘below’’ and ‘‘right’’, C) The observed attention patterns can be induced by positional embedding.

specified spatial relation, indicating that the head transmits shape identity independently of relational context (Fig. 5A). During sampling, in contrast to **spatial relation head**, this communication channel is active later in sampling (step 4–8), linking each objects to their corresponding shape tokens in the prompt (Fig. 5B).

#### 4.4. Ablation and causal manipulation

To test whether the heads discussed above have a causal role in correct spatial relation and object shape generation, we perform both ablation and causal manipulation experiments.

First, we perform head-specific ablation of cross-attention. Specifically, we remove the contribution from a specific cross-attention head on either the spatial relation (Fig. 6A) or object (Fig. 6B) text tokens. Ablating spatial-

relation attention specifically in L2H8 reduces relational accuracy from 67% to 33%, while other heads show negligible effects (Fig. 6A). This confirms L2H8’s critical role in implementing the correct spatial layout. On the other hand, ablating cross-attention to the object text in specifically L4H3 decreases the object shape generation accuracy from 90% to 76%, while the ablation of other layer head combinations shows minimal effect (Fig. 6B). This emphasized the critical value of such a head in robustly generating the correct object shape. Although the effect size of object shape ablation is smaller than that of spatial relations ablation, the effects in both cases are confined only to the two previously identified heads, L2H8 and L4H3, suggesting a highly concentrated circuit.

We reason that L2H8 and L4H3 functions in sequence

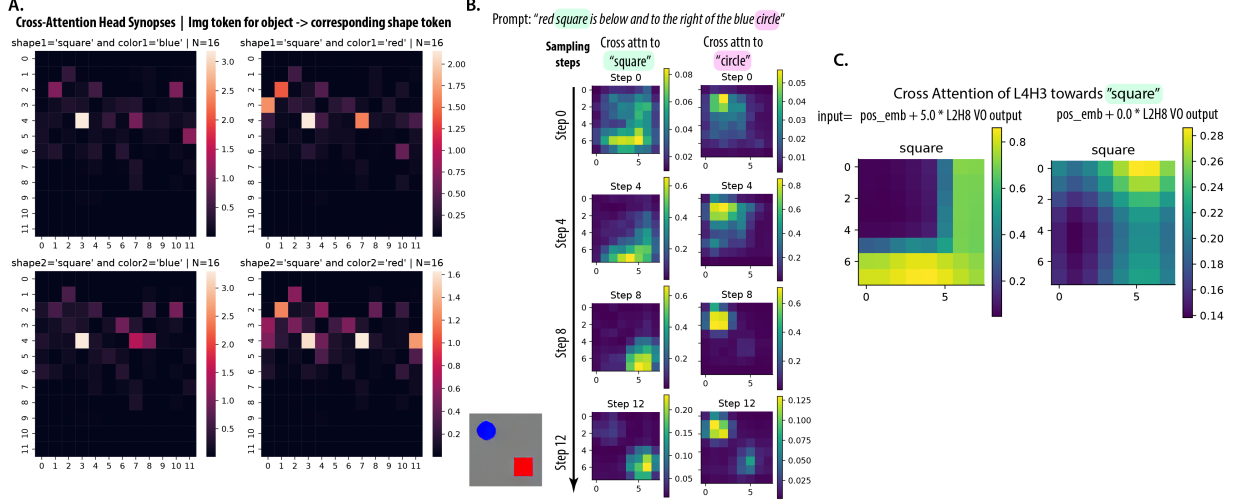


Figure 5. **The object generation heads in random-embedding-based T2I.** **A)** We find specialized heads in the synopses of cross-attention, computed from image tokens of each object to its own shape tokens. **B)** We show the activation of this head across images tokens and sampling steps for the prompt “red square is below and to the right of the blue circle”: tokens at the eventual square location attend to “square,” while the other object attends to “circle”; selectivity sharpens from Step 0→12. **C)** Injecting the VO output of the relation head (L2H8) into positional embeddings is sufficient to elicit selective attention from tagged locations to the “square” token (left); without the tag the pattern is weak (right). This indicates the object generation head reads the relational tag generated by the spatial relation head.

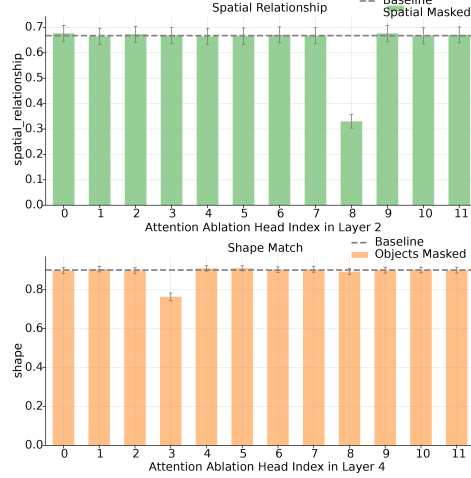


Figure 6. **Attention head ablation** reveals focused effect of L2H8 on spatial relation and L4H3 on object shape.

to generate a correct object at the correct spatial location. To test this hypothesis, we inject the VO output of the relation head (L2H8) into the object generation head’s (L4H3) image tokens positional embeddings. This manipulation is sufficient to elicit selective attention from tagged locations to the “square” token (Fig. 5C). Without the injected VO inputs, no obvious attention pattern is observed (right), showing that the downstream object shape head reads the relational tag.

**Consistency across model sizes** Finally, we assess whether this circuit mechanism generalizes across RTE-DiT

models of different sizes (App. A.3). We find the spatial relation heads consistently emerge in DiT of three scales (DiT-B, mini, micro). In contrast, the smallest model (DiT-nano) shows no such head and performs poorly on spatial relation (accuracy 5%) (Tab. 2).

**Summary** Taking it together, for DiTs trained with random token embedding (RTE), relational object generation unfolds in two stages (Fig. 7): the “**spatial relation head**” reads relational text tokens (e.g., “above,” “left”) via the QK circuit and interact with the sinusoidal positional encoding of image tokens, producing spatial gradients for each relation. The VO circuit writes positional tags (e.g., Tag 1) onto image tokens, marking where the object (e.g. 1st in sentence) should appear. In the “**object generation head**”, tokens with matching tags attend to shape token of the corresponding object. The VO circuit maps these text features (e.g., “square”, “circle”) into visual features at tagged locations, generating the object via denoising.

This modularizes operation where relation heads laying the ground and object heads assigning attributes provides a clean and disentangled mechanism for robust composition of relation and object combination.

## 5. Relation circuits in T5-DiT

Given the clear mechanism found in RTE-based T2I models, we then apply the same *Attention Synopsis* method and identify specialized cross attention heads for spatial relation in T5-based models. However, no clear pattern emerges

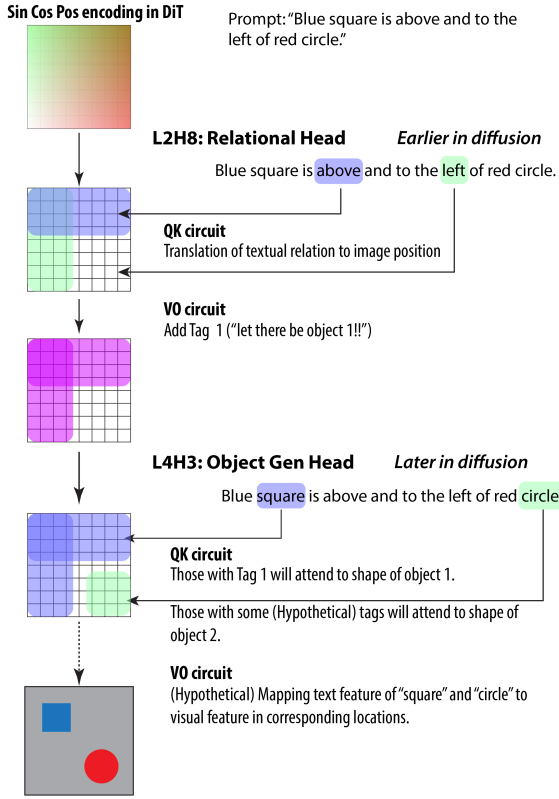


Figure 7. Schematics of the object relation circuit in DiT trained with random embedding

from averaging (App. A.5), suggesting that T5-DiT could be using alternative mechanisms.

**T5-DiT extracts relations from other tokens** We note that, via the T5 encoder’s self-attention, each text token could absorb information from the entire sentence, one hypothesis is that the image tokens may receive the spatial relation information from non-relation tokens. We test this hypothesis by performing attention masking on text tokens to see which one has the largest ablation effect on relational object generation (Fig. 8A). Surprisingly, the relation words, filler and color words have little effect on the generation performance (Fig. 8A). Ablating `<end_of_sentence>` token disrupts the denoising generation process, leading to a collapse of all evaluation metrics. The relation accuracy decreases after masking shape1 and shape2, where ablating shape1 reduces spatial relation by 15%, while ablating shape2 harms all shape, binding and relation accuracy by 50%.

This ablation result could explain the absence of relation and object generation attention head. Through T5 encoder, the information of object1 and object2 and their relation has been encoded in the contextual embedding of shape2 and shape1 tokens, thus DiT only needs to decode the information from them to achieve successful generations, making

its attention to relation words weak and noisy.

### Structure of relation representation in T5 embedding

This mixture of semantic information is further confirmed by visualization (UMAP, tSNE, PCA) of the T5 contextual embedding of the second shape token ( $V_{\text{shape2}}^*$ ). All visualizations consistently show clear qualitative separation by spatial relation and, within each relation, by object2’s color (Fig. 23). This indicates that multiple factors—its own identity, the other object’s identity, and the spatial relation—are jointly represented in this embedding space.

We further analyze this effect by a variance partition analysis (App.B.6). We model the contextual embedding of the second object token as a linear combination of four factor vectors:  $V_{\text{shape2}}^* = V_{\text{shape2}} + V_{\text{color2}} + V_{\text{shape1}} + V_{\text{rel}}$ . This structure allows us to extract a vector for each level within a factor (e.g., a vector for “upper right” versus “lower left”), enabling controlled embedding manipulations. Variance partitioning supports this factorization (Tab. 1). In the raw T5 embedding, shape2 accounts for the largest share of variance ( $\sim 37.5\%$  partial  $R^2$ ), with relation still contributing substantially ( $\sim 12\%$ ). After projection through the DiT MLP, the balance shifts: relation becomes the dominant factor ( $\sim 21\%$ ), while shape2’s share decreases, suggesting DiTs reorganize the token representation and amplify the relation information for generation.

		$V_{\text{shape2}}$	$V_{\text{color2}}$	$V_{\text{shape1}}$	$V_{\text{rel}}$	tot. $R^2$
T5 emb	part. $R^2$	37.5%	4.7%	5.0%	12.1%	73.2%
	marg. $R^2$	51.4%	4.7%	18.9%	12.1%	
DiT MLP	part. $R^2$	14.9%	8.0%	7.2%	21.3%	53.4%
	marg. $R^2$	16.9%	8.0%	9.0%	21.3%	

Table 1. Variance partitioning of T5 embedding and DiT-MLP projection of shape2 token.

**Control relational object generation** To causally test the hypothesis that relation information is encoded in specific object tokens within the T5 embedding, we performed targeted vector arithmetic on the 4096-d prompt embedding for a shape token (e.g., “square”). Starting from the original embedding of object2, (e.g.  $V_{\text{square}}^*$  in prompt “blue circle is to the lower left of red square”), we subtracted the learned factor vector for the original relation (e.g.,  $V_{\text{lower left}}$ ) and added a scaled vector for an alternative relation (e.g.,  $2V_{\text{lower right}}$  or  $2V_{\text{upper right}}$ ).

As shown in Fig. 8B, this manipulation systematically shifts the generated object positions to match the new relational configuration, while leaving object identities (color and shape) largely intact. This provides direct causal evidence that relational geometry is embedded in the contextual representation of the shape2 token, and that simple linear operations in this space can reconfigure spatial relations

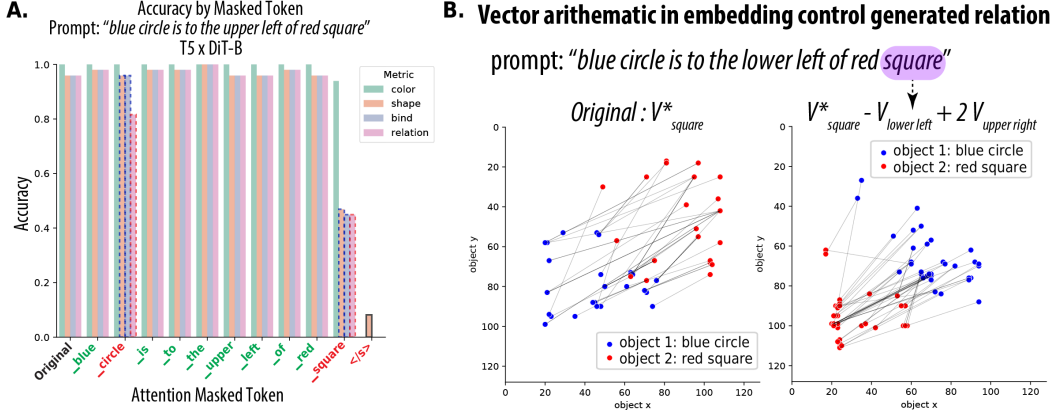


Figure 8. **Mechanism for relational generation in T5-DiT.** **A.** T5-based DiT is robust to attention ablation of relation word, but most sensitive to shape2 and EOS. **B.** Manipulation via factorized word vector arithmetic causally affects generated object relation.

in generated images.

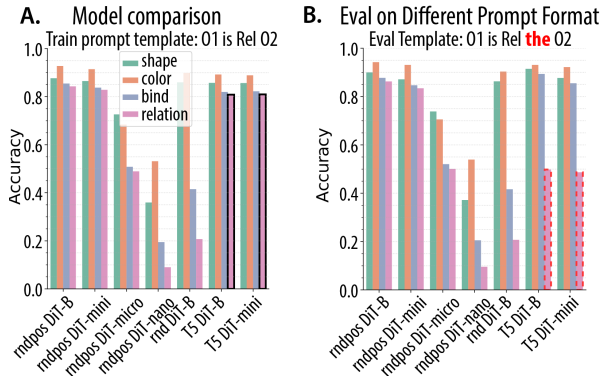


Figure 9. **Evaluation of model performance on trained and generalized prompt template.**

**Robustness of RTE-based and T5-based circuits** When evaluating on prompt with the exact format as the training ones, RTE- and T5-trained models have comparably high performance on spatial relation. However, slight prompt variation breaks the tie, i.e. adding *the* to the prompt reduces the relational accuracy of T5-DiT model by around 40% (Fig. 9B., Tab. 2). This suggests that even though the task accuracies are similar between RTE-based and T5-based T2I models, their robustness to the small perturbations in the text is different. The T5-based model is more sensitive to the perturbation, likely because altered context shifts token embeddings away from the learned directions used by its cross-attention and MLP layers.

## 6. Discussion

We find that Diffusion Transformers can learn to generate scenes with correct object–relation composition when trained on a minimalistic relational dataset, but the underlying mechanisms depend strongly on the choice of text en-

coder. Both T5 and RTE encoding models achieve high relational accuracy, yet they differ markedly in their attention circuits, their generalization behavior, and their sensitivity to perturbations.

RTE-DiTs are highly sensitive to relational words ablation yet robust to filler word changes. In contrast, T5-DiT models are robust to relational word ablation but sensitive to small lexical variations, indicating that explicit relation tokens play a limited role in their generation. These differences in generation properties can be linked to their distinctive attention circuit mechanisms. RTE-DiT models use a modularized strategy: a specialized “relational heads” directly read and translate relation tokens into spatial gradients across image tokens, guiding object placement before identity assignment; then a separate object generate head places the objects according to the spatial gradients. T5-DiT models instead use an object-centric strategy: contextual embeddings from T5 absorb relational information into object tokens (especially the last shape words), allowing both spatial layout and single object attribute to be decoded from one or two token embeddings. This approach is more compact but less disentangled, and sensitive to small perturbation of the two token embedding, even due to addition of nuisance words.

These results highlight that text embedding design shapes not only performance but also inductive bias and interpretability. RTE enables explicit, object-invariant, disentangled relation-to-location pathways, offering clearer control mechanisms, while T5 embeddings promote integration of relational cues into object features, potentially aiding linguistic generalization but obscuring intermediate relational processing. The trade-off between interpretability, prompt robustness, and reliance on explicit relational tokens should inform future text-to-image model design.

### **Acknowledgments**

We gratefully acknowledge support from the Kempner Research Fellowship (B.W.) and the Schwartz Fellowship (X.P.), as well as computing resources provided by the Kempner Institute cluster. We thank Martin Wattenberg, Yonatan Belinkov, and Thomas Fel for their careful reading and valuable feedback on earlier versions of this work. We also appreciate the insightful comments and discussion from participants and reviewers of the New England Mechanistic Interpretability (NEMI) Workshop and the Mechanistic Interpretability Workshop at NeurIPS 2025.

## References

[1] Michael S. Albergo, Nicholas M. Boffi, and Eric Vanden-Eijnden. Stochastic Interpolants: A Unifying Framework for Flows and Diffusions, 2023. 1

[2] Gary Bradski. The opencv library. *Dr. Dobb's Journal of Software Tools*, 2000. 3

[3] Agneet Chatterjee, Gabriela Ben Melech Stan, Estelle Aftalo, Sayak Paul, Dhruba Ghosh, Tejas Gokhale, Ludwig Schmidt, Hannaneh Hajishirzi, Vasudev Lal, Chitta Baral, and Yezhou Yang. Getting it right: Improving spatial consistency in text-to-image models, 2024. 1

[4] Hila Chefer, Yuval Alaluf, Yael Vinker, Lior Wolf, and Daniel Cohen-Or. Attend-and-excite: Attention-based semantic guidance for text-to-image diffusion models, 2023. 1, 2

[5] Junsong Chen, Jincheng Yu, Chongjian Ge, Lewei Yao, Enze Xie, Yue Wu, Zhongdao Wang, James Kwok, Ping Luo, Huchuan Lu, and Zhenguo Li. PixArt-\$\alpha\$: Fast Training of Diffusion Transformer for Photorealistic Text-to-Image Synthesis, 2023. 2, 3, 25

[6] Colin Conwell and Tomer Ullman. Testing Relational Understanding in Text-Guided Image Generation, 2022. 1

[7] Prafulla Dhariwal and Alex Nichol. Diffusion Models Beat GANs on Image Synthesis. <https://arxiv.org/abs/2105.05233v4>, 2021. 1

[8] Nelson Elhage, Neel Nanda, Catherine Olsson, Tom Henighan, Nicholas Joseph, Ben Mann, Amanda Askell, Yuntao Bai, Anna Chen, Tom Conerly, Nova Das-Sarma, Dawn Drain, Deep Ganguli, Zac Hatfield-Dodds, Danny Hernandez, Andy Jones, Jackson Kernion, Liane Lovitt, Kamal Ndousse, Dario Amodei, Tom Brown, Jack Clark, Jared Kaplan, Sam McCandlish, and Chris Olah. A mathematical framework for transformer circuits. *Transformer Circuits Thread*, 2021. <https://transformercircuits.pub/2021/framework/index.html>. 4

[9] Dhruba Ghosh, Hanna Hajishirzi, and Ludwig Schmidt. Geneval: An object-focused framework for evaluating text-to-image alignment, 2023. 1

[10] Xu Han, Linghao Jin, Xiaofeng Liu, and Paul Pu Liang. Progressive compositionality in text-to-image generative models. In *The Thirteenth International Conference on Learning Representations*, 2025. 1

[11] Amir Hertz, Ron Mokady, Jay Tenenbaum, Kfir Aberman, Yael Pritch, and Daniel Cohen-Or. Prompt-to-prompt image editing with cross attention control. *arXiv preprint arXiv:2208.01626*, 2022. 4

[12] Jonathan Ho and Tim Salimans. Classifier-free diffusion guidance. *arXiv preprint arXiv:2207.12598*, 2022. 3, 26

[13] Jonathan Ho, Ajay Jain, and Pieter Abbeel. Denoising diffusion probabilistic models. *Advances in Neural Information Processing Systems*, 33:6840–6851, 2020. 1

[14] Jonathan Ho, Tim Salimans, Alexey Gritsenko, William Chan, Mohammad Norouzi, and David J Fleet. Video diffusion models. In *Advances in Neural Information Processing Systems*, pages 8633–8646. Curran Associates, Inc., 2022. 1

[15] Kaiyi Huang, Kaiyue Sun, Enze Xie, Zhenguo Li, and Xihui Liu. T2i-combench: A comprehensive benchmark for open-world compositional text-to-image generation. *Advances in Neural Information Processing Systems*, 36:78723–78747, 2023. 1

[16] Kaiyi Huang, Chengqi Duan, Kaiyue Sun, Enze Xie, Zhenguo Li, and Xihui Liu. T2I-CompBench++: An Enhanced and Comprehensive Benchmark for Compositional Text-to-Image Generation. *IEEE Transactions on Pattern Analysis and Machine Intelligence*, (01):1–17, 2025. 1

[17] Raphi Kang, Yue Song, Georgia Gkioxari, and Pietro Perona. Is clip ideal? no. can we fix it? yes!, 2025. 2

[18] Tero Karras, Miika Aittala, Jaakko Lehtinen, Janne Hellsten, Timo Aila, and Samuli Laine. Analyzing and Improving the Training Dynamics of Diffusion Models, 2024. 3

[19] Yuheng Li, Haotian Liu, Qingyang Wu, Fangzhou Mu, Jianwei Yang, Jianfeng Gao, Chunyuan Li, and Yong Jae Lee. Gligen: Open-set grounded text-to-image generation, 2023. 1

[20] Yaron Lipman, Ricky T. Q. Chen, Heli Ben-Hamu, Maximilian Nickel, and Matt Le. Flow Matching for Generative Modeling, 2023. 1

[21] Bingyan Liu, Chengyu Wang, Tingfeng Cao, Kui Jia, and Jun Huang. Towards Understanding Cross and Self-Attention in Stable Diffusion for Text-Guided Image Editing, 2024. *arXiv:2403.03431 [cs]*. 4

[22] Cheng Lu, Yuhao Zhou, Fan Bao, Jianfei Chen, Chongxuan Li, and Jun Zhu. Dpm-solver++: Fast solver for guided sampling of diffusion probabilistic models. *arXiv preprint arXiv:2211.01095*, 2022. 3, 26

[23] Maya Okawa, Ekdeep Singh Lubana, Robert P. Dick, and Hidenori Tanaka. Compositional Abilities Emerge Multiplicatively: Exploring Diffusion Models on a Synthetic Task, 2024. 2

[24] Core Francisco Park, Maya Okawa, Andrew Lee, Hidenori Tanaka, and Ekdeep Singh Lubana. Emergence of Hidden Capabilities: Exploring Learning Dynamics in Concept Space, 2024. 2

[25] Quynh Phung, Songwei Ge, and Jia-Bin Huang. Grounded text-to-image synthesis with attention refocusing, 2023. 2

[26] Colin Raffel, Noam Shazeer, Adam Roberts, Katherine Lee, Sharan Narang, Michael Matena, Yanqi Zhou, Wei Li, and Peter J. Liu. Exploring the Limits of Transfer Learning with a Unified Text-to-Text Transformer, 2023. 3

[27] Robin Rombach, Andreas Blattmann, Dominik Lorenz, Patrick Esser, and Björn Ommer. High-Resolution Image Synthesis with Latent Diffusion Models, 2022. 2, 3

[28] Robin Rombach, Andreas Blattmann, Dominik Lorenz, Patrick Esser, and Björn Ommer. High-resolution image synthesis with latent diffusion models. In *Proceedings of the IEEE/CVF Conference on Computer Vision and Pattern Recognition*, pages 10684–10695, 2022. 1, 25

[29] Jascha Sohl-Dickstein, Eric Weiss, Niru Maheswaranathan, and Surya Ganguli. Deep unsupervised learning using nonequilibrium thermodynamics. In *Proceedings of the 32nd International Conference on Machine Learning*, pages 2256–2265, Lille, France, 2015. PMLR. 1

[30] Raphael Tang, Akshat Pandey, Zhiying Jiang, Gefei Yang, Karun Kumar, Jimmy Lin, and Ferhan Ture. What the

DAAM: Interpreting stable diffusion using cross attention.  
*arXiv preprint arXiv:2210.04885*, 2022. [4](#)

[31] Martin Wattenberg and Fernanda B. Viégas. Relational Composition in Neural Networks: A Survey and Call to Action, 2024. [2](#)

[32] Enze Xie, Junsong Chen, Junyu Chen, Han Cai, Haotian Tang, Yujun Lin, Zhekai Zhang, Muyang Li, Ligeng Zhu, Yao Lu, and Song Han. SANA: Efficient High-Resolution Image Synthesis with Linear Diffusion Transformers, 2024. [2](#)

[33] Gaoyang Zhang, Bingtao Fu, Qingnan Fan, Qi Zhang, Runxing Liu, Hong Gu, Huaqi Zhang, and Xinguo Liu. Compass: Enhancing spatial understanding in text-to-image diffusion models, 2024. [2](#)

## A. Extended Results

### A.1. Evaluation and Benchmark

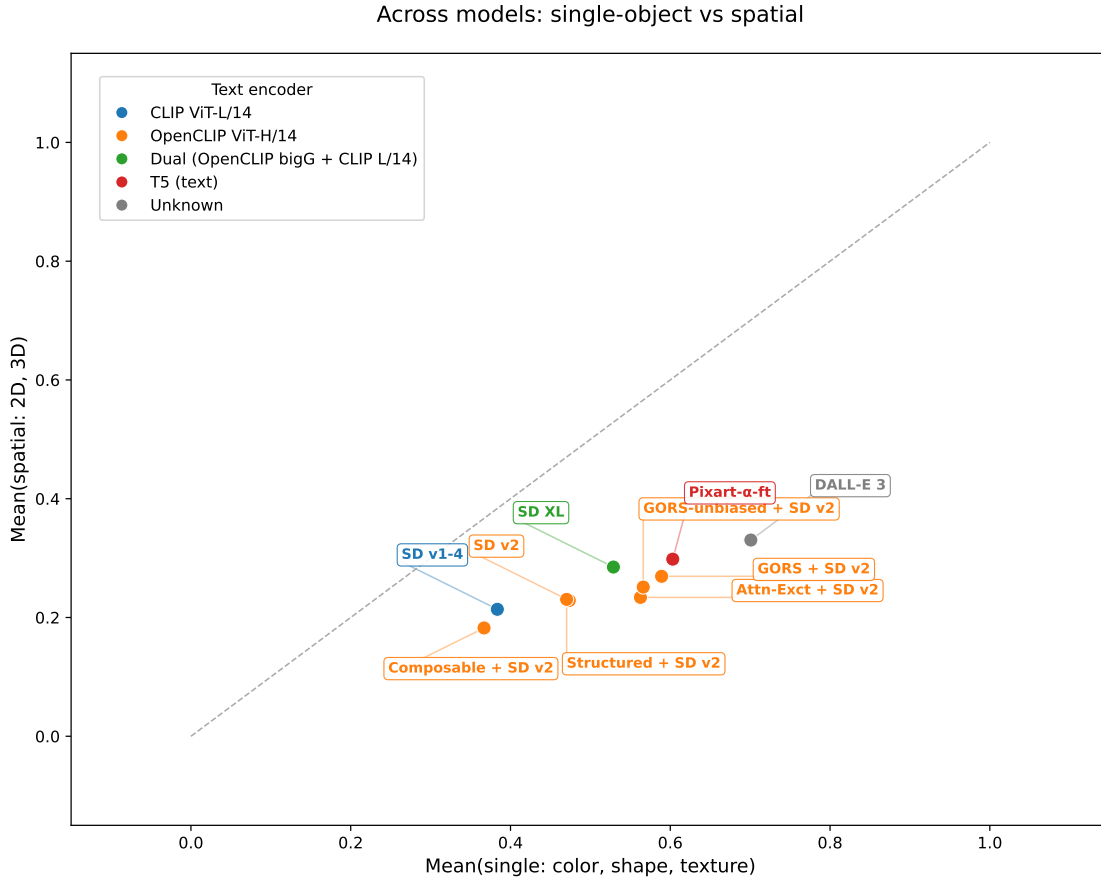


Figure 10. **Benchmark scores of spatial relationship and object feature attributes of open and closed source model** Color of dots denote the text encoder.

Table 2. **Comprehensive evaluation of models on prompt template variations.**

**Abbreviations:** WD: weight decay, rnd: random embedding, rndpos: random embedding plus position encoding. *bind*: unique and correct attribute binding. *sp rel*: spatial relation correctness (loose). *sp rel+*: spatial relation correctness (stringent). *Dx*, *Dy*: difference of coordinates between the two identified objects (with target attributes  $x_1 - x_2$ ,  $y_1 - y_2$ , with the unit pixel (128 pixel total). All statistics are averaged from 264 prompts, covering all 8 relations and all object combinations, each drawing 50 samples. Thus, the non-zero value in *Dx*, *Dy* suggests systematic bias in spatial relation.

model name	template	shape	color	bind	sp rel	sp rel+	Dx	Dy
rndpos DiT-B	O1 is Rel O2	0.877	0.928	0.855	0.843	0.758	-0.4	-0.9
	O1 is Rel the O2	0.900	0.942	0.877	0.862	0.717	-0.3	-0.4
	O1 Rel O2	0.858	0.909	0.833	0.823	0.752	-1.2	-1.6
	O1 Rel the O2	0.877	0.925	0.853	0.842	0.759	-0.3	-1.2
	the O1 is Rel the O2	0.895	0.946	0.868	0.833	0.614	-0.9	0.5
rndpos DiT-mini	O1 is Rel O2	0.865	0.914	0.838	0.828	0.644	0.8	0.4
	O1 is Rel the O2	0.871	0.931	0.847	0.834	0.613	1.1	1.5
	O1 Rel O2	0.778	0.845	0.743	0.737	0.621	1.5	-0.4
	O1 Rel the O2	0.799	0.879	0.770	0.762	0.616	1.8	0.0
	the O1 is Rel the O2	0.767	0.912	0.721	0.680	0.471	-0.1	1.8
rndpos DiT-micro	O1 is Rel O2	0.726	0.683	0.508	0.489	0.315	-0.2	0.2
	O1 is Rel the O2	0.738	0.705	0.520	0.501	0.312	0.3	0.2
	O1 Rel O2	0.626	0.604	0.395	0.386	0.270	0.1	-1.5
	O1 Rel the O2	0.649	0.639	0.410	0.401	0.269	-0.2	-1.2
	the O1 is Rel the O2	0.665	0.724	0.432	0.403	0.234	2.1	-0.7
rndpos DiT-nano	O1 is Rel O2	0.360	0.531	0.195	0.090	0.049	3.2	-0.1
	O1 is Rel the O2	0.372	0.539	0.205	0.096	0.051	2.4	-1.6
	O1 Rel O2	0.270	0.568	0.146	0.069	0.037	5.1	-0.4
	O1 Rel the O2	0.279	0.581	0.151	0.071	0.036	3.2	-2.4
	the O1 is Rel the O2	0.399	0.632	0.193	0.082	0.047	-3.6	-3.5
rnd DiT-B	O1 is Rel O2	0.859	0.899	0.415	0.207	0.192	-0.1	0.1
	O1 is Rel the O2	0.863	0.903	0.416	0.207	0.190	-0.0	-0.0
	O1 Rel O2	0.856	0.893	0.412	0.205	0.191	0.0	-0.0
	O1 Rel the O2	0.860	0.902	0.415	0.206	0.191	-0.0	0.1
	the O1 is Rel the O2	0.866	0.910	0.417	0.207	0.188	0.1	0.0
T5 DiT-B	O1 is Rel O2	0.857	0.892	0.820	0.808	0.749	-0.8	-0.5
	O1 is Rel the O2	0.915	0.931	0.894	0.498	0.306	-33.7	-24.9
	O1 Rel O2	0.853	0.871	0.825	0.608	0.493	-4.5	-16.6
	O1 Rel the O2	0.941	0.958	0.925	0.400	0.217	-35.1	-37.0
	the O1 is Rel the O2	0.917	0.935	0.896	0.529	0.309	-18.4	-20.7
T5 DiT-mini	O1 is Rel O2	0.856	0.889	0.822	0.810	0.659	-0.4	-0.6
	O1 is Rel the O2	0.877	0.922	0.855	0.487	0.259	-35.8	-24.1
	O1 Rel O2	0.816	0.844	0.772	0.559	0.399	-12.7	-18.2
	O1 Rel the O2	0.895	0.946	0.878	0.391	0.184	-38.7	-37.6
	the O1 is Rel the O2	0.906	0.947	0.885	0.537	0.272	-17.1	-19.3
T5 DiT-B WD	O1 is Rel O2	0.183	0.114	0.033	0.033	0.031	-1.2	1.3
	O1 is Rel the O2	0.169	0.104	0.030	0.017	0.013	-39.7	-22.2
	O1 Rel O2	0.164	0.110	0.032	0.025	0.023	-5.0	-15.4
	O1 Rel the O2	0.181	0.122	0.037	0.016	0.011	-40.4	-34.8
	the O1 is Rel the O2	0.160	0.100	0.028	0.017	0.013	-15.0	-18.4
T5 DiT-mini WD	O1 is Rel O2	0.894	0.942	0.866	0.854	0.667	-0.4	1.0
	O1 is Rel the O2	0.911	0.967	0.886	0.521	0.265	-42.0	-19.1
	O1 Rel O2	0.843	0.886	0.804	0.596	0.429	-9.1	-16.7
	O1 Rel the O2	0.911	0.975	0.888	0.414	0.189	-47.1	-35.3
	the O1 is Rel the O2	0.911	0.965	0.887	0.514	0.249	-22.4	-13.8

## A.2. Evaluation Training Dynamics

Prompt: “blue triangle is to the upper left of red square” 14 steps, cfg 4.5

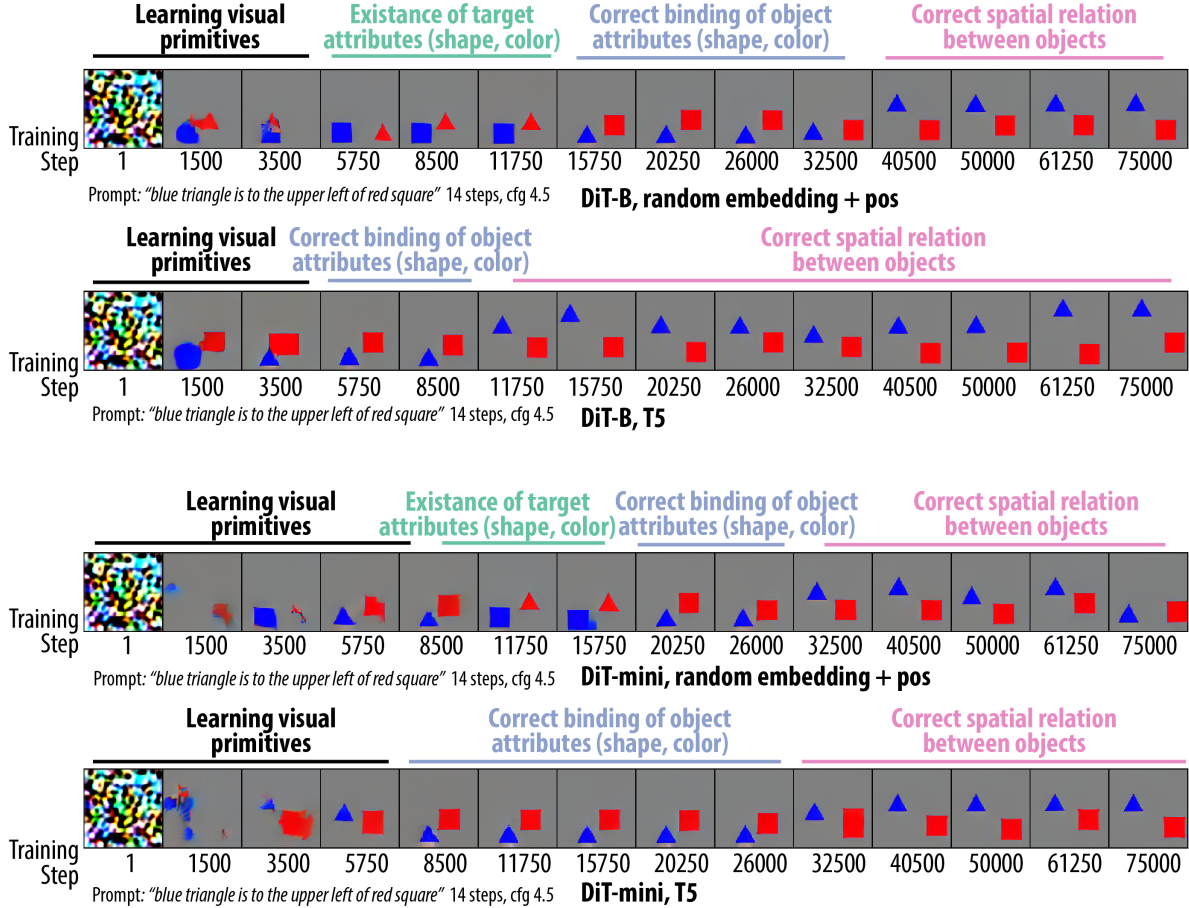


Figure 11. **Comparison of training dynamics of DiT models with different text encoding and scale.** Specific evaluation prompt used was “blue triangle is to the upper left of red square”, sampled with 14 steps at cfg 4.5, sampled from the same noise seed. Further, T5 models immediately learn to achieve object attribute binding after learning attributes themselves, while random embedding model gradually learn the correct attribute binding and then spatial relation. Across scales, generally, larger scale models train faster.

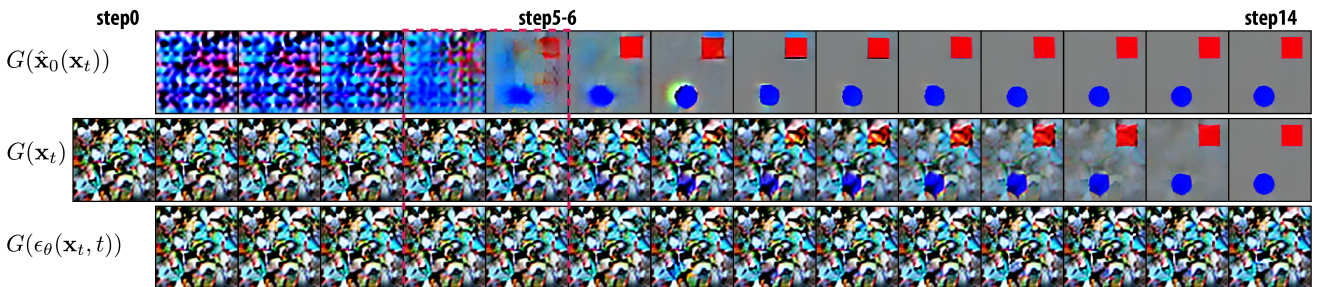


Figure 12. **Observation on sampling dynamics** Specific evaluation prompt used was “the red square is above and to the right of the blue circle”, sampled with 14 steps at cfg 4.5. Model used is DiT-B rand emb pos. A transition can be seen at step 4-6, where the two object at their final positions can be clearly seen from the expected outcome  $G(\hat{x}_0(x_t))$ .

### A.3. RTE-DiT Spatial Relation Head Additional Evidence

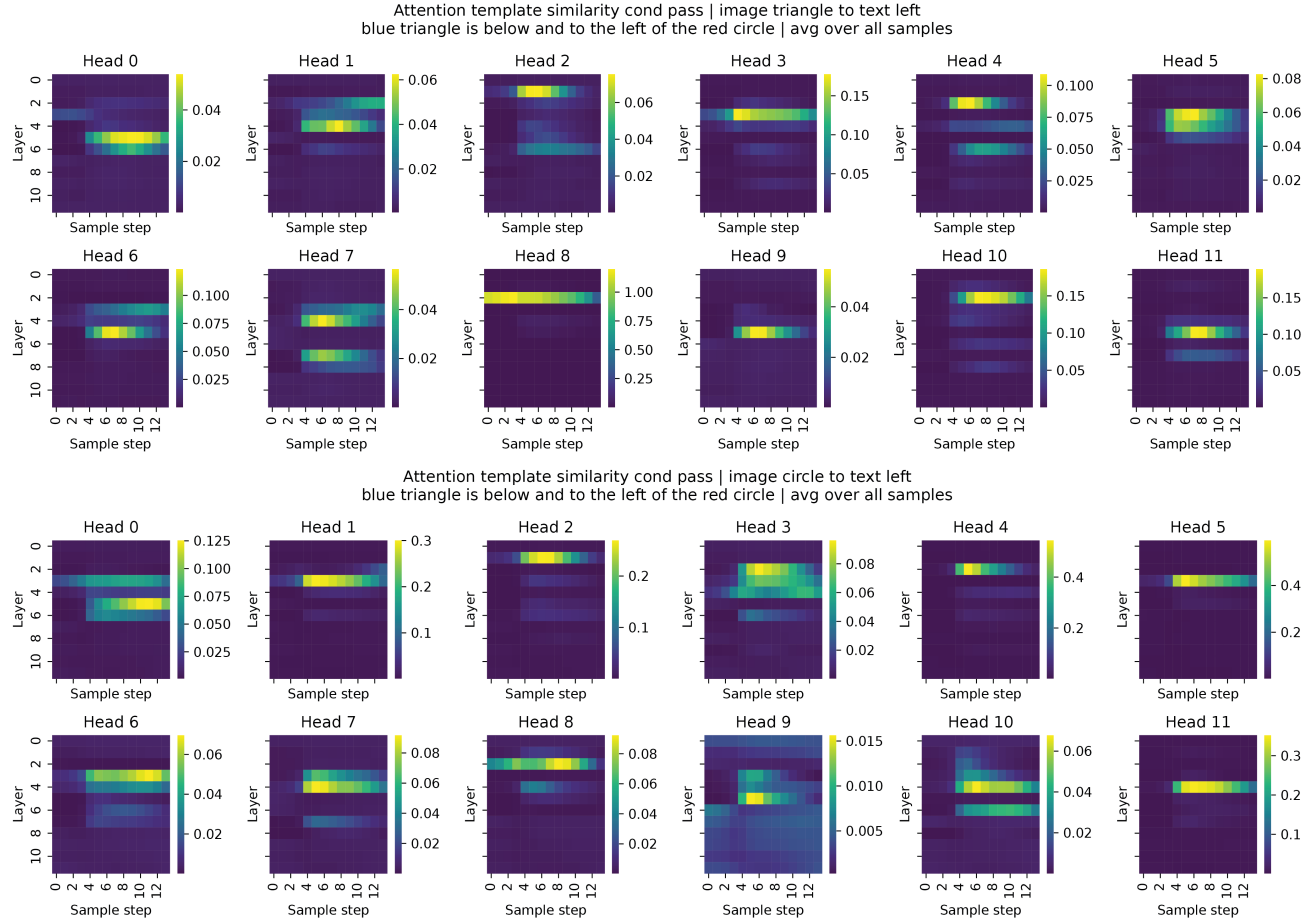


Figure 13. **Cross attention energy during sampling dynamics.** Highlighting the smooth varying attention strength, and the salient contribution of L2H8 head from first object to relation words.

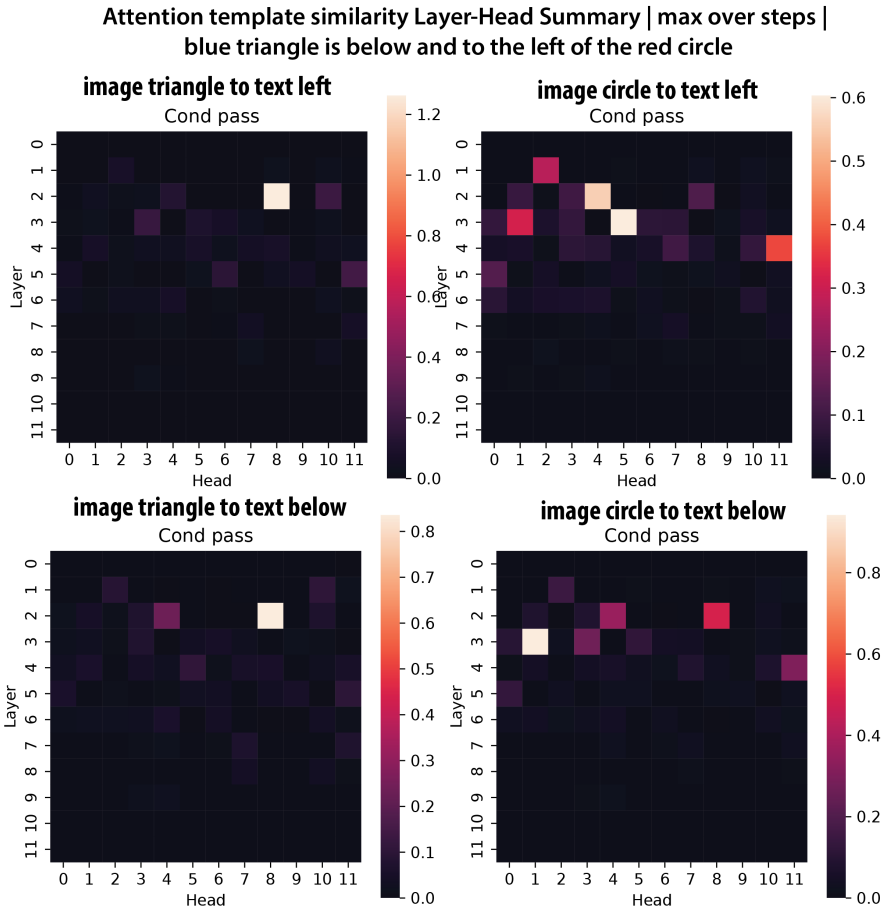


Figure 14. Cross attention energy summary (max over time) for the prompt above

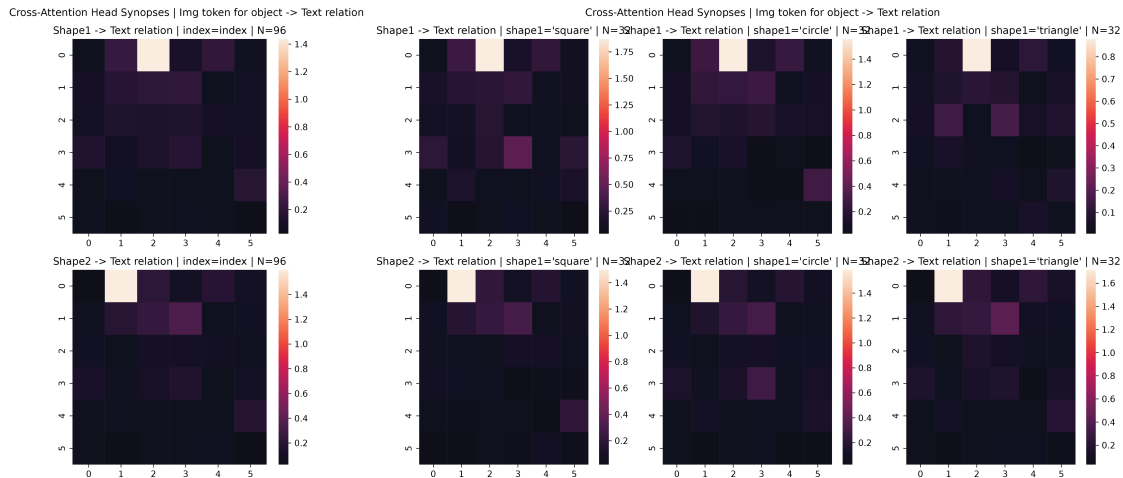


Figure 15. Attention Synopsis for Shape to Relation word for DiT-mini, showing it's invariant to the specific shape of object1.

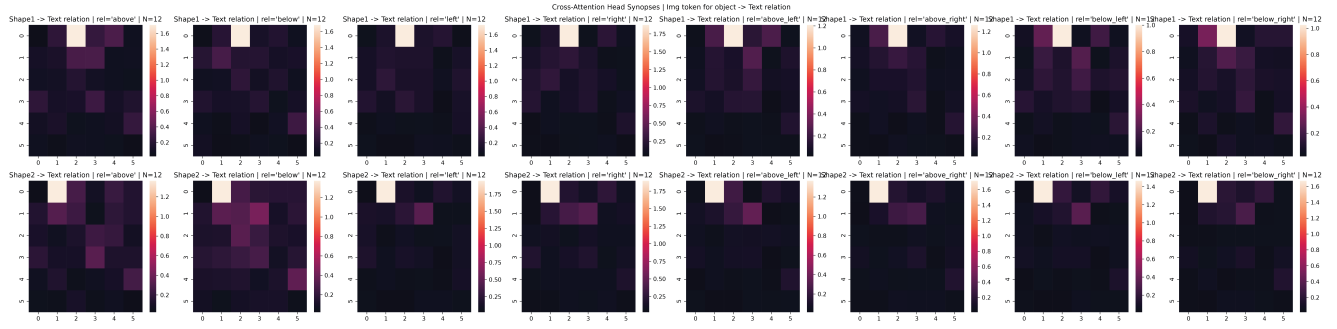


Figure 16. Attention Synopsis for Shape to Relation word for DiT-mini, showing it's invariant to the specific spatial relation and phrasing.

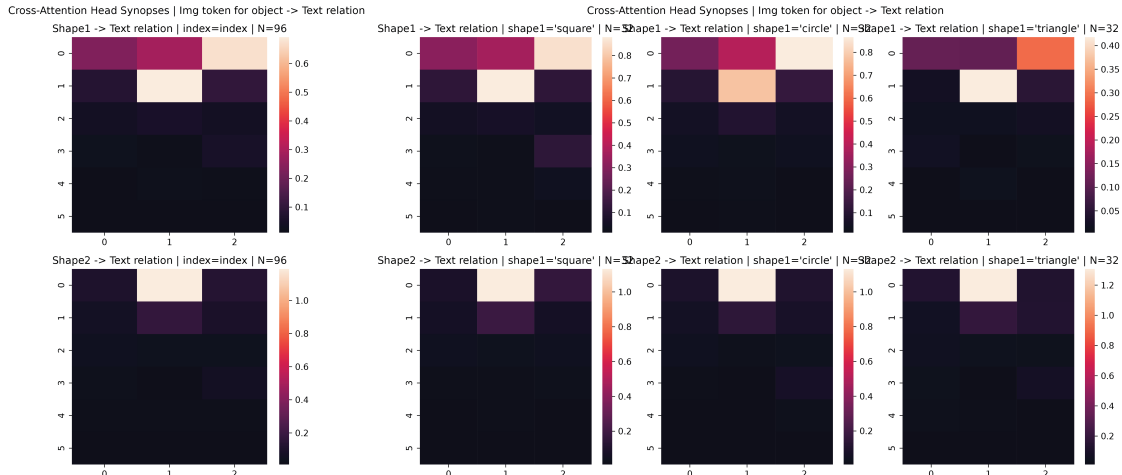


Figure 17. Attention Synopsis for Shape to Relation word for DiT-micro, showing it's invariant to the specific shape of object1.

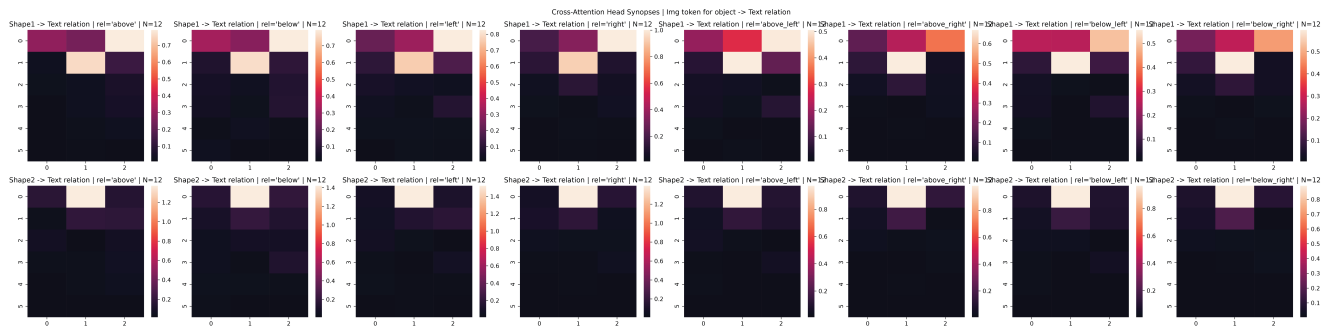


Figure 18. Attention Synopsis for Shape to Relation word for DiT-micro, showing it's invariant to the specific spatial relation and phrasing.

#### A.4. RTE-DiT Object Head Additional Evidence

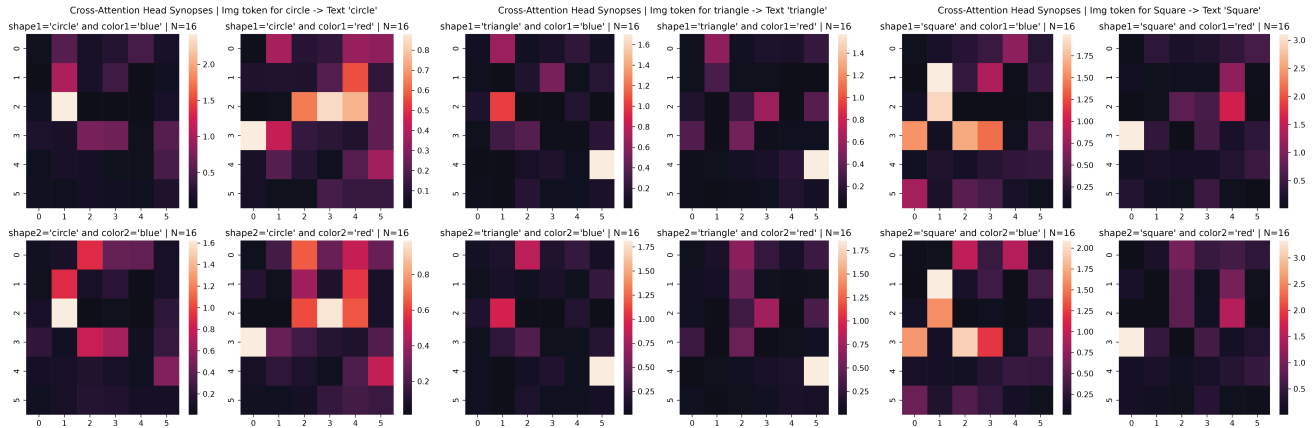


Figure 19. Attention Synopsis for Shape to corresponding shape word for DiT-mini.

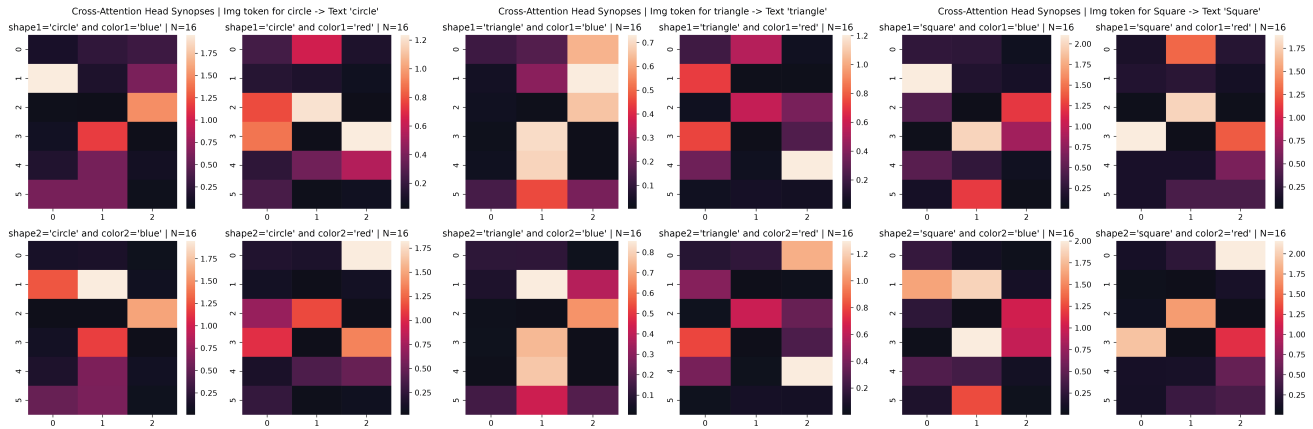


Figure 20. Attention Synopsis for Shape to corresponding Shape word for DiT-micro.

## A.5. T5-DiT Attention Synopsis

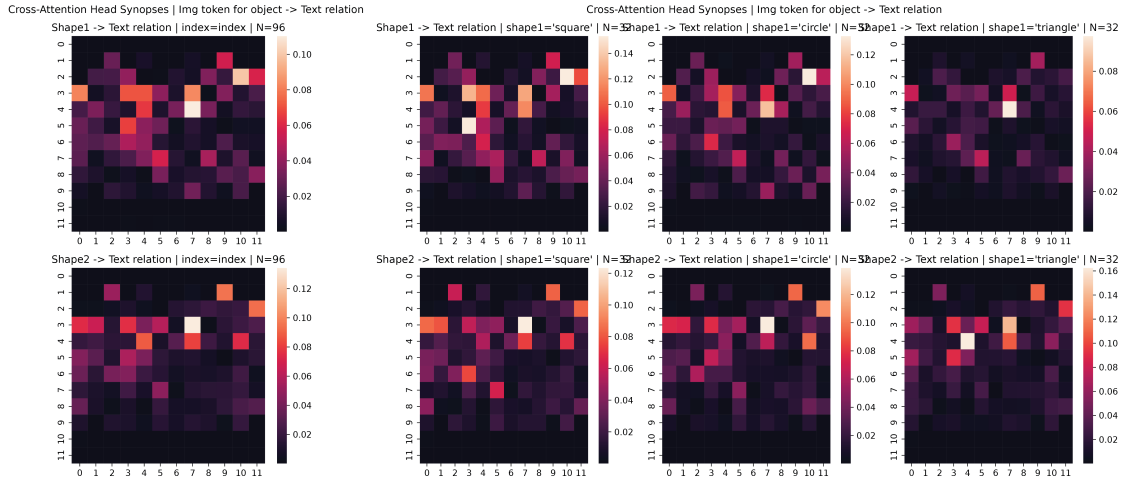


Figure 21. Attention Synopsis for Shape to Relation word for DiT-B with T5 encoding. The pattern is much less clear than RTE.

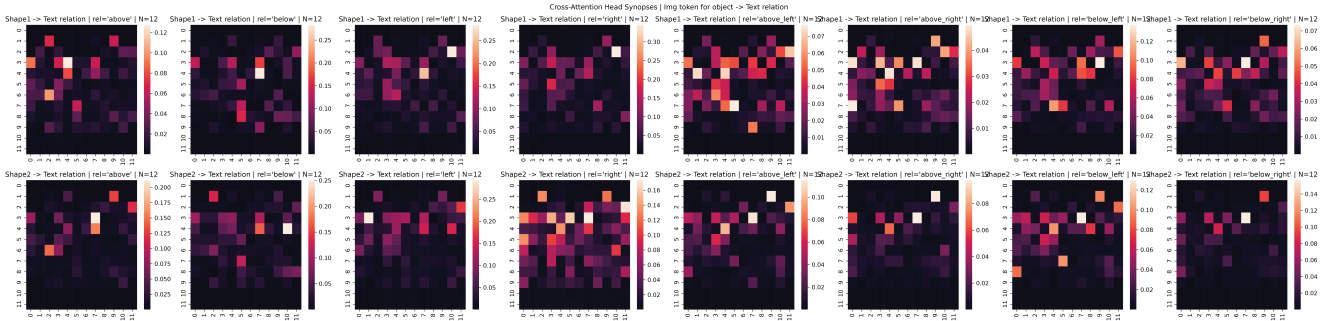
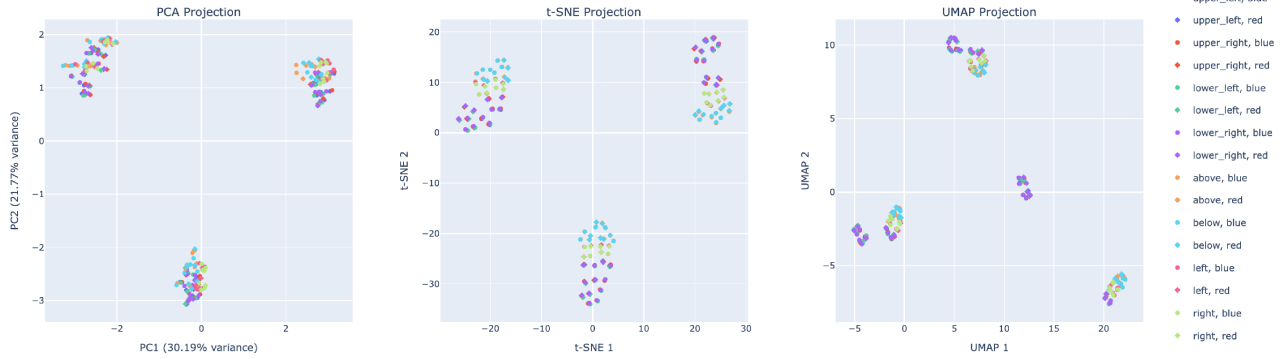


Figure 22. Attention Synopsis for Shape to Relation word for DiT-B with T5 encoding. The pattern is much less clear than RTE.

## A.6. T5-DiT Representation Analysis

### T5 contextual embedding of shape2 token



### DiT-MLP projection of T5 embedding of shape2 token

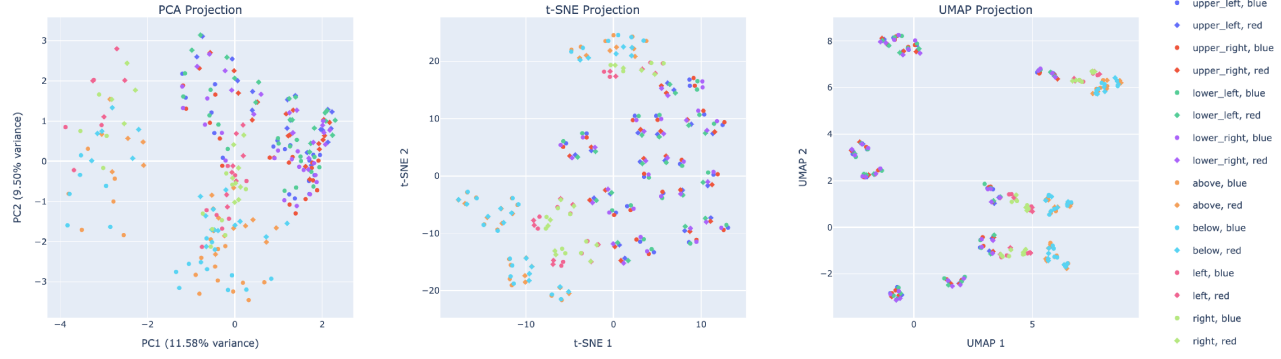


Figure 23. Dimension reduction visualization of shape2 token representation (PCA, tSNE, UMAP). Top row: T5 contextual embedding (4096d), Bottom row: DiT-MLP projection (784d).

## B. Detailed Method

### B.1. Object-Relation Dataset Construction

To study spatial reasoning under controlled conditions, we generate a synthetic dataset of paired images and natural-language captions. Each sample contains two objects rendered on a uniform gray background at a resolution of  $128 \times 128$  pixels. Here we describe the generative process of the image and text pair, basically, we first sample the images and then generate the captions accordingly. For details of generation logic, see the pseudo code below.

**Image Rendering.** For each image, we randomly sample two *distinct* shapes from  $\{\text{circle}, \text{square}, \text{triangle}\}$  with order, and call them  $\text{shape1}$  and  $\text{shape2}$ . Consequently, there are 6 possible combinations of  $(\text{shape1}, \text{shape2})$ . Then we place them at uniformly sampled coordinates

$$(x_i, y_i) \sim \mathcal{U}(r+1, 128-r-1), \quad i = 1, 2,$$

where  $r = 16$  is the radius (or half-side length) controlling object scale. Circles and squares are drawn using their canonical analytic outlines, while triangles are equilateral with side length  $2r$ . To disambiguate the objects, we set them as different colors, one blue and one red. Without loss of generality, the first-selected shape is rendered in **red** and the second in **blue**. To produce controlled occlusion events, the drawing order is determined by a fair coin flip; the last-drawn object is considered visually “in front.”

**Occlusion Detection.** We compute axis-aligned bounding boxes  $B_1$  and  $B_2$  for the two shapes and evaluate their intersection area

$$A_{\text{overlap}} = \text{area}(B_1 \cap B_2).$$

If the normalized overlap exceeds a 5% threshold,

$$\frac{A_{\text{overlap}}}{\min(\text{area}(B_1), \text{area}(B_2))} > 0.05,$$

we label the objects as occluding. In such cases, the spatial relationship is determined by the rendering order: the topmost shape is “in front of” the other.

**Spatial-Relation Annotation.** When no significant occlusion occurs, spatial relations are assigned analytically from the relative positions of the two shape centers. Using a 5-pixel tolerance, we assign a spatial relation by comparing the centers  $(x_1, y_1)$  and  $(x_2, y_2)$  of the two shapes. If  $|x_1 - x_2| \leq 5$ , the relation is classified as *above* or *below* depending on the sign of  $y_1 - y_2$ . If  $|y_1 - y_2| \leq 5$ , it is classified as *left of* or *right of*. Otherwise, the relation falls into one of the four diagonal categories (*upper-left*, *upper-right*, *lower-left*, *lower-right*), determined jointly by the signs of  $(x_1 - x_2)$  and  $(y_1 - y_2)$ .

**Caption Generation.** For each image, we generate a natural language caption that describes the relationship of the  $\text{shape1}$  relative to the  $\text{shape2}$  using the geometric and occlusion labels described above.

If the two shapes are occluding, we select either an “in front of” or “behind” relation according to the rendering order. A paraphrase variant is then sampled uniformly at random from the corresponding set of templates (e.g., “in front of,” “overlapping and in front of,” “behind,” “overlapped by”, see Tab. 3).

When no occlusion is present, the captioning module uses the categorical relation (above/below/left/right/diagonal) derived above from  $(x_1, y_1)$  and  $(x_2, y_2)$  and uniformly maps it to one of several paraphrases (Tab. 3). To introduce controlled linguistic variation while preserving semantic structure, we optionally prepend color modifiers to each shape. Concretely, the first and second shapes are associated with fixed colors (**red** and **blue**), and for each caption we randomly decide whether to include the color adjective or omit it for each shape (50% chance).

The final caption is produced in a template of the form

$$\text{“[shape1] is [relation] [shape2]”,}$$

with optional color modifiers and paraphrased relational expressions

$$\text{“[color1] [shape1] is [relation] [color2] [shape2]”,}$$

. Example captions produced by the system include:

- “square is in front of triangle.”
- “red triangle is above blue circle.”
- “red circle is overlapped by blue triangle.”
- “red square is to the lower left of blue triangle.”
- “square is left of triangle.”
- “square is to the right of blue triangle.”
- “circle is diagonally up and left from square.”
- “circle is below and to the left of triangle.”
- “red triangle is diagonally down and left from square.”
- “circle is higher than blue triangle.”

**Dataset Output.** For each of the 10,000 generated samples, we store: (i) the rendered RGB image, (ii) shape identities, (iii) pixel coordinates, (iv) occlusion state and depth order, (v) the categorical spatial–relation label, and (vi) the corresponding caption. This dataset provides a controlled setting for evaluating multi-object scene generation.

Relation	Paraphrase Variants
upper_left	to the upper left of; above and to the left of; diagonally up and left from
upper_right	to the upper right of; above and to the right of; diagonally up and right from
lower_left	to the lower left of; below and to the left of; diagonally down and left from
lower_right	to the lower right of; below and to the right of; diagonally down and right from
above	above; directly above; higher than
below	below; directly below; lower than
left	to the left of; left of
right	to the right of; right of
in_front	in front of; overlapping and in front of
behind	behind; overlapped by

Table 3. Paraphrase templates for each spatial relation used in caption generation.

```

def generate_sample(canvas_size=128, radius=16):
    """Generate one synthetic example: image, labels, and caption."""
    shapes = ["triangle", "circle", "square"]
    colors = {1: "red", 2: "blue"} # shape1, shape2
    # 1. Sample two distinct shapes
    shape1, shape2 = sample_two_distinct(shapes)
    # 2. Sample valid positions (inside canvas margins)
    x1, y1 = sample_position(canvas_size, radius)
    x2, y2 = sample_position(canvas_size, radius)
    # 3. Randomize drawing order (decides which shape is visually on top)
    draw_order = random.choice([(shape1, (x1, y1), 1), (shape2, (x2, y2), 2)])
    if draw_order[0] == shape1:
        # draw shape2 then shape1
        draw_shape(shape2, (x2, y2), color=colors[2])
        draw_shape(shape1, (x1, y1), color=colors[1])
        shape1_on_top = True
    else:
        # draw shape1 then shape2
        draw_shape(shape1, (x1, y1), color=colors[1])
        draw_shape(shape2, (x2, y2), color=colors[2])
        shape1_on_top = False

    # 4. Compute occlusion via bounding boxes
    box1 = get_shape_bbox(shape1, (x1, y1), radius)
    box2 = get_shape_bbox(shape2, (x2, y2), radius)
    overlap_ratio = overlap_area(box1, box2) / min(area(box1), area(box2))
    if overlap_ratio > 0.05:
        # Significant occlusion
        if shape1_on_top:
            relation_key = "in_front"
        else:
            relation_key = "behind"
    else:
        # 5. Geometric relation from relative centers
        dx = x1 - x2
        dy = y1 - y2
        tol = 5
        if abs(dx) <= tol:
            relation_key = "above" if dy < 0 else "below"
        elif abs(dy) <= tol:
            relation_key = "left" if dx < 0 else "right"
        else:
            if dx < 0 and dy < 0:
                relation_key = "upper_left"
            elif dx < 0 and dy > 0:
                relation_key = "lower_left"
            elif dx > 0 and dy < 0:
                relation_key = "upper_right"
            else:
                relation_key = "lower_right"
    # 6. Sample natural-language phrase for this relation
    phrase = random.choice(SPATIAL_PHRASES[relation_key])
    # Optionally include or drop color adjectives
    shape1_qual = random.choice([colors[1], ""])
    shape2_qual = random.choice([colors[2], ""])
    # 7. Compose caption: "<shape1> is <relation> <shape2>"
    caption = f"{shape1_qual} {shape1} is {phrase} {shape2_qual} {shape2}".strip()
    # 8. Return image and labels (shape ids, positions, relation, caption, etc.)
    labels = {
        "shape1": shape_to_idx(shape1),
        "shape2": shape_to_idx(shape2),
        "location1": (x1, y1),
        "location2": (x2, y2),
        "spatial_relationship": relation_key,
        "caption": caption,
    }
    return image, labels

```

## B.2. Model Architecture and Training

### B.2.1. Text Encoders

We experiment with two kinds of text encoders as conditioning of T2I model: (i) a pretrained T5 encoder and (ii) randomized embedding baselines (with and without positional encodings). All setups share a common tokenization.

**Tokenization.** Captions are tokenized with a T5 tokenizer using a fixed maximum sequence length of  $L = 20$  tokens. For each caption  $c$ , we apply padding and truncation to obtain input IDs and attention masks:

$$\text{tokenizer}(c, \text{max\_length} = L, \text{padding} = \text{'max\_length'}, \text{truncation} = \text{True}).$$

We additionally construct an “unconditional” prompt by tokenizing the empty string  $c = \text{''''}$ , which is used as the null-conditioning input (e.g., for classifier-free guidance).

**Pretrained T5 Encoder.** The default text encoder is a T5EncoderModel from the pretrained `t5-v1.1-xxl` checkpoint. We load the encoder at mixed precision (bffloat16) and treat it as a *frozen* feature extractor. For a tokenized prompt  $(\text{input\_ids}, \text{attention\_mask})$ , the encoder produces a sequence of contextual embeddings  $E \in \mathbb{R}^{L \times D}$ , where  $D = 4096$  is the hidden dimension for T5-XXL.

**Random Embedding Baselines.** To disentangle the role of true linguistic structure from that of generic token-level conditioning, we also employ randomized text encoders that replace the T5 encoder with fixed random embeddings. Both variants operate on a learned-free dictionary

$$\text{embedding\_dict} \in \mathbb{R}^{V' \times D},$$

where  $V'$  is the number of distinct token IDs appearing in the caption corpus and  $D = 4096$  matches the dimensionality of the T5-XXL encoder.

To construct this dictionary, we first gather all unique token IDs from the tokenized captions. Given the token matrix  $\text{input\_ids\_tsr} \in \mathbb{N}^{N \times L}$ , we compute

$$\text{unique\_input\_ids} = \text{Unique}(\text{input\_ids\_tsr}),$$

and retain the inverse mapping needed to reconstruct the full caption tensor. For each unique token ID, we then sample a random embedding vector

$$e_i \sim \mathcal{N}\left(0, \frac{7.5^2}{D} I_D\right), \quad i = 1, \dots, |\text{unique\_input\_ids}|.$$

The scaling factor 7.5 is chosen to approximately match the empirical  $\ell_2$  norm of T5-XXL embeddings, ensuring that the resulting random encoders operate in a comparable magnitude regime and that the diffusion model receives conditioning vectors of the correct scale.

The resulting matrix

$$\text{embedding\_dict} \in \mathbb{R}^{|\text{unique\_input\_ids}| \times D}$$

is paired with two lookup tables,

$$\text{input\_ids2dict\_ids} : \mathbb{N} \rightarrow \{0, \dots, V' - 1\}, \quad \text{dict\_ids2input\_ids} : \{0, \dots, V' - 1\} \rightarrow \mathbb{N},$$

which implement a deterministic one-to-one mapping between tokenizer IDs and dictionary rows. These components are cached and used identically across all random-embedding text encoder variants.

**RandomEmbeddingEncoder without Positional Encoding.** The first baseline, replaces the T5 encoder with a simple embedding lookup layer. Given token IDs  $x \in \mathbb{N}^L$ , we map each ID to its dictionary index and retrieve the corresponding embedding:

$$E_t = \text{embedding\_dict}[\text{input\_ids2dict\_ids}(x_t)], \quad t = 1, \dots, L.$$

No positional encodings or contextualization are applied; each token is represented by an independent random vector. The resulting embedding tensor has shape  $L \times D$  and is used in place of T5 features.

**RandomEmbeddingEncoder with Positional Encodings.** The second baseline, RandomEmbeddingEncoder\_wPosEmb, augments the random embeddings with sinusoidal positional encodings. We construct a standard transformer-style positional encoding  $\text{wpe} \in \mathbb{R}^{L \times D}$  using sine and cosine functions with logarithmically spaced frequencies:

$$\text{wpe}_{t,2k} = \sin\left(\frac{t}{10000^{2k/D}}\right), \quad \text{wpe}_{t,2k+1} = \cos\left(\frac{t}{10000^{2k/D}}\right),$$

for positions  $t = 0, \dots, L - 1$  and feature indices  $k$ . The positional encodings are scaled by a factor of  $1/6$  and added to the random embeddings:

$$\tilde{E}_t = E_t + \alpha \cdot \text{wpe}_t, \quad \alpha = \frac{1}{6}.$$

This yields position-aware random features with the same shape and dtype as the T5 embeddings, enabling a drop-in replacement while preserving the position information for each language token.

Together, these three configurations—pretrained T5, random embeddings without position, and random embeddings with sinusoidal positional encodings—allow us to probe how much of the text2image generative model’s performance depends on rich linguistic structure versus generic token-level conditioning signals.

### B.2.2. Image Encoders

Following the original PixArt framework [5], we use the pretrained variational autoencoder (VAE) from Stable Diffusion [28] (sd-vae-ft-ema) as our image encoder. The VAE downsamples the spatial resolution by a factor of 8 in each dimension and produces a 4-channel latent representation.

### B.2.3. Diffusion Transformer

We set the patch size of DiT as 2, which results in  $8 \times 8 = 64$  image tokens per latent. We use the PixArt backbone with:

- no windowed attention (`window_size=0, window_block_indexes=[]`),
- no relative positional encoding (`use_rel_pos=False`),
- full-precision attention layers enabled (`fp32_attention=True`),
- transformer context length of 20 (`model_max_length=20`).

We train a family of PixArt backbones with different scales, that differ in transformer depth, hidden size, and number of attention heads (all use patch size 2). PixArt\_B\_2 uses 12 layers with a 768-dimensional hidden size and 12 heads. PixArt\_S\_2 retains the 12-layer depth but reduces the hidden size to 384 with 6 heads. The smaller PixArt\_mini\_2 and PixArt\_micro\_2 variants use 6 layers with hidden sizes of 384 and 192, respectively, each with 6 or 3 heads. The most compact model, PixArt.nano\_2, uses 3 layers with a 192-dimensional hidden size and 3 heads. Together, these variants allow us to systematically examine how object–relation learning and circuit solutions scale with model capacity.

### B.2.4. Training

We train the PixArt model on our synthetic dataset using the configuration shown below. Unless otherwise noted, we follow the standard PixArt training setup with several adjustments to accommodate our text encoders and small image resolution (128×128). The key hyperparameters are summarized below.

**Data and Input Format.** Images are encoded with the Stable Diffusion VAE, producing  $4 \times 16 \times 16$  latent tensors. Captions are tokenized to a maximum length of 20 tokens, and conditioning embeddings have dimensionality 4096. The caption embedding and image latents are pre-computed to reduce training overhead.

**Optimization.** The model is trained using AdamW with learning rate  $1 \times 10^{-4}$ , weight decay  $3 \times 10^{-2}$ , and  $\epsilon = 10^{-10}$ . A constant learning-rate schedule with 500 warmup steps is applied, and gradient clipping is set to 0.01.

**Training Schedule and Batch Size.** We train for up to 4000 epochs with a global batch size of 256, resulting in 160000 gradient steps. No gradient accumulation is used (`gradient_accumulation_steps=1`), and gradient checkpointing is enabled to reduce memory usage. During training, samples for a set of validation prompts are periodically generated to check the training status.

Overall, the most critical hyperparameters for our experiments are the large batch size (256), the AdamW configuration (`lr 1e-4, wd 3e-2`), the short context length (20 tokens).

### B.3. Sampling

We generate images using a DPM-solver++[22] sampler with 14 inference steps for fast generation. We use classifier-free guidance [12] with a scale of 4.5 to strengthen the conditional signal.

### B.4. Evaluation

We evaluate models on their ability to (i) correctly generate object-level structure and (ii) satisfy a parametric scene description specifying shapes, colors, and spatial relations. To this end, we implement a deterministic analysis pipeline that parses each generated image into object hypotheses and compares them against the ground-truth scene specification.

**Object Parsing and Classification.** Given a generated image, we first convert it to a NumPy array and process each color channel independently using OpenCV. For each channel, we threshold the intensity at 180 to obtain a binary mask, extract connected components via contour detection, and approximate each contour using `cv2.approxPolyDP`. The resulting polygon is classified as a *triangle*, *square*, or *circle* based on its number of vertices (3, 4, or  $> 4$ , respectively). We discard small components whose area falls below a fixed threshold (100 pixels). For each surviving contour, we compute: (i) the shape label, (ii) the bounding box and center coordinates, (iii) the contour area, and (iv) the mean RGB color over the contour region, yielding a DataFrame of detected objects.

Color identities (*red* vs. *blue*) are derived by thresholding the mean RGB values: an object is tagged as red-dominant if its red channel is near 255 and the green and blue channels are near zero (within a margin of 25), and analogously for blue-dominant. This produces binary indicators `is_red` and `is_blue` used for subsequent matching.

**Canonical Spatial Relation from Detections.** To recover the spatial relation between two detected objects, we use their center coordinates  $(x_1, y_1)$  and  $(x_2, y_2)$ . We define  $\Delta x = x_1 - x_2$  (positive when object 1 is to the right of object 2) and  $\Delta y = y_1 - y_2$  (positive when object 1 is lower in the image). Using a 5-pixel tolerance, we map  $(\Delta x, \Delta y)$  to one of eight discrete relations: *above*, *below*, *left*, *right*, *upper\_left*, *upper\_right*, *lower\_left*, *lower\_right*. Vertical alignment ( $|\Delta x| \leq 5$ ) yields *above* or *below*, horizontal alignment ( $|\Delta y| \leq 5$ ) yields *left* or *right*, and all other cases are assigned to one of the four diagonal categories according to the signs of  $(\Delta x, \Delta y)$ .

**Parametric Query Evaluation.** Each scene is paired with a parametric description

```
scene_info = (shape1, shape2, color1, color2, spatial_relationship),
```

which encodes the intended relation “shape1 of color1 is spatial\_relationship shape2 of color2.” For a given detection DataFrame, we construct two candidate sets:

- $O_1$ : objects whose shape matches `shape1` and whose color satisfies `color1`
- $O_2$ : analogously for `shape2` and `color2`.

We then compute the following indicators: (i) *shape correctness*: whether the two required shapes (if specified) exist in the detection set, (ii) *color correctness*: whether the two required colors (if specified) exist, (iii) *existence of a valid binding*: whether  $O_1$  and  $O_2$  are both non-empty, and (iv) *uniqueness*: whether there is exactly one object in each set ( $|O_1| = |O_2| = 1$ ).

When a unique binding is present, we extract the centers of the matched objects, compute  $(\Delta x, \Delta y)$ , and infer the observed spatial relation using the deterministic mapping above. A strict spatial-relation score is obtained by checking whether the observed relation exactly matches `spatial_relationship`.

**Strict and Loose Spatial Criteria.** In addition to the strict criterion, we define a looser spatial correctness measure that tolerates deviations within a larger margin and we relax the directional constraint by also accepting diagonally oriented configurations (e.g., *above-right*) as valid instances of ‘*above*’ or ‘*right*’. Specifically, we apply relation-specific inequalities on  $(\Delta x, \Delta y)$  with threshold (default 8 pixels). For example, an “*above*” relation is considered correct if  $\Delta y < -\text{threshold}$ , while an “*upper\_right*” relation is satisfied if  $\Delta x > \text{threshold}$  and  $\Delta y < -\text{threshold}$ . This yields a binary `spatial_relationship_loose` flag. In main text, the spatial relation accuracy is computed from this `spatial_relationship_loose` flag.

**Metrics.** For each image–scene pair, the evaluation function returns a set of diagnostic booleans: `shape`, `color`, `exist_binding`, `unique_binding`, `spatial_relationship`, and `spatial_relationship_loose`, as well as the overall scores

$$\begin{aligned} \text{overall} &= \text{shape} \wedge \text{color} \wedge \text{unique\_binding} \wedge \text{spatial\_relationship}, \\ \text{overall\_loose} &= \text{shape} \wedge \text{color} \wedge \text{unique\_binding} \wedge \text{spatial\_relationship\_loose}. \end{aligned}$$

We additionally record the raw offsets ( $\Delta x, \Delta y$ ) and the absolute coordinates of the two matched objects, which we use for diagnostic plots and ablations. These metrics allow us to separately quantify failures in object identity, color binding, and spatial configuration, as well as to report a single binary success indicator per prompt.

## B.5. Attention Map Synopsis

To understand how different PixArt models encode object–relation prompts, we perform a detailed analysis of cross-attention activations during generation. Our procedure instruments the PixArt transformer with custom attention processors that record all self-attention and cross-attention maps at every denoising step. For each prompt, we generate  $N = 49$  images using  $T = 14$  inference steps and collect the full tensor

$$\mathbf{A}^{\text{cross}} \in \mathbb{R}^{L \times T \times (2N) \times H \times S \times W},$$

where  $L$  is the number of transformer blocks,  $T$  is the number of denoising steps,  $2N$  is the total number of samples,  $H$  is the number of attention heads, and  $S$  and  $W$  denote image and text-token dimensions respectively. The first  $N$  samples correspond to unconditional run (classifier-free guidance), and the latter  $N$  correspond to conditional run; we analyze these separately.

**Object-Based Image Masks.** To relate attention patterns to generated content, we extract object masks for each image using a contour-based CV2 pipeline. Each image is decomposed into binary masks for *square*, *triangle*, *circle*, and *background* regions. Masks are resized to the attention resolution (typically  $8 \times 8$ ) and normalized to obtain an image-token mask  $\mathbf{M}^{\text{img}} \in [0, 1]^{N \times S}$ . Note this mask differs per samples, since object appears on different locations. This allows us to pool attention contributions associated with specific generated objects.

**Text-Token Masks.** For each prompt, we tokenize the caption using the T5 tokenizer and construct multi-hot masks over text tokens for various semantic groups (e.g., `{square}`, `{triangle}`, `{above}`, `{left}`, `{red}`, `{blue}`, or function words `{and, to, the, of}`). This yields text-token masks  $\mathbf{M}^{\text{text}} \in \{0, 1\}^W$ , which allow selective measurement of attention into any subset of words.

**Template Similarity Scoring.** Given an image-token mask and text-token mask, we construct an outer-product template

$$\mathbf{T} = \mathbf{M}^{\text{img}} \otimes \mathbf{M}^{\text{text}} \in \mathbb{R}^{N \times S \times W},$$

which highlights cross-attention positions connecting a specific visual region to a specific group of words. The cross-attention activation  $\mathbf{A}^{\text{cross}}$  is then scored by computing

$$\text{Score}_{\ell, t, h} = \sum_{i, j} \mathbf{A}_{\ell, t, h}^{\text{cross}}(i, j) \mathbf{T}(i, j),$$

yielding a tensor of size  $L \times T \times H$ . These scores are computed separately for the conditional and unconditional branches.

**Layer-Head Synopsis and Visualization.** For each prompt and each (image-mask, text-mask) pair, we summarize the scores by either: (1) aggregating across inference steps (max or mean), or (2) selecting the maximum-activation step per head. Heatmaps over layers and heads visualize where the model most strongly aligns specific visual regions with specific words. We additionally report the top- $k$  heads per prompt, showing which attention heads—and at which layers—encode relations such as “square  $\leftrightarrow$  left” or “triangle  $\leftrightarrow$  above.”

**Prompt Sweep.** We evaluate all 168 possible binary spatial-relation prompts (all color/shape combinations crossed with 8 relation types). For each prompt, we generate images, extract masks, compute cross-attention templates, visualize layer-head activation maps, and save summary statistics along with the best-performing heads. This produces a full synopsis of how relation semantics are distributed across layers, heads, and denoising steps for each trained model.

## B.6. Variance Partition and Factorization

Let  $\{\mathbf{x}_i\}_{i=1}^n, \mathbf{x}_i \in \mathbb{R}^d$ , denote the representations of  $n$  samples (e.g., embedding vectors) arranged in a matrix

$$X = \begin{bmatrix} \mathbf{x}_1^\top \\ \vdots \\ \mathbf{x}_n^\top \end{bmatrix} \in \mathbb{R}^{n \times d}. \quad (1)$$

Each sample is annotated by a set of categorical factors (features)  $f \in \mathcal{F}$ , such as spatial relationship or shape1. For a given factor  $f$ , we denote the label of stimulus  $i$  by  $y_i^{(f)} \in \{1, \dots, L_f\}$ , where  $L_f$  is the number of levels of that factor.

**Centered design matrices.** For each categorical factor  $f$  we construct a one-hot design matrix  $Z^{(f)} \in \mathbb{R}^{n \times L_f}$ ,

$$Z_{i\ell}^{(f)} = \begin{cases} 1 & \text{if } y_i^{(f)} = \ell, \\ 0 & \text{otherwise,} \end{cases} \quad (2)$$

and remove the intercept by column-centering

$$Z^{(f)} \leftarrow Z^{(f)} - \frac{1}{n} \mathbf{1} \mathbf{1}^\top Z^{(f)}, \quad (3)$$

where  $\mathbf{1} \in \mathbb{R}^n$  is the all-ones vector. We then concatenate all factors into a single design matrix

$$Z = [Z^{(f_1)} \mid Z^{(f_2)} \mid \dots \mid Z^{(f_{|\mathcal{F}|})}] \in \mathbb{R}^{n \times p}. \quad (4)$$

**Metric Gram matrix.** We analyze variance in a (possibly nonlinear) feature space induced by a distance or similarity metric on  $X$ . Let

$$J_n = I_n - \frac{1}{n} \mathbf{1} \mathbf{1}^\top \quad (5)$$

be the centering matrix. Depending on the metric, we construct a centered Gram matrix  $A \in \mathbb{R}^{n \times n}$ :

- **Euclidean metric.** For the standard Euclidean geometry, we center  $X$  across samples and form

$$X_c = J_n X, \quad A = X_c X_c^\top. \quad (6)$$

This is equivalent to the standard linear kernel on centered features.

- **General dissimilarity metrics.** For a generic metric  $\delta(\mathbf{x}_i, \mathbf{x}_j)$ , we form the pairwise distance matrix  $D \in \mathbb{R}^{n \times n}$ ,  $D_{ij} = \delta(\mathbf{x}_i, \mathbf{x}_j)$ , and its elementwise square  $D^{\circ 2}$ , then apply classical multidimensional scaling (MDS) centering:

$$A = -\frac{1}{2} J_n D^{\circ 2} J_n. \quad (7)$$

The matrix  $A$  can be interpreted as the centered inner-product matrix in an implicit feature space associated with the chosen metric. Its total variance is

$$SS_{\text{total}} = \text{tr}(A). \quad (8)$$

**Projection operators and total explained variance.** Given the full design matrix  $Z$ , we define the orthogonal projector onto its column space as

$$P_{\text{all}} = Z (Z^\top Z)^+ Z^\top, \quad (9)$$

where  $(\cdot)^+$  denotes the Moore–Penrose pseudoinverse. In practice we compute  $P_{\text{all}}$  via a rank-revealing QR decomposition and discard numerically degenerate directions for robustness.

The residual projector is  $P_\perp = I_n - P_{\text{all}}$ . We then define

$$SS_{\text{resid}} = \text{tr}(AP_\perp), \quad (10)$$

$$SS_{\text{model}} = SS_{\text{total}} - SS_{\text{resid}}, \quad (11)$$

and the overall coefficient of determination

$$R_{\text{total}}^2 = \frac{SS_{\text{model}}}{SS_{\text{total}}}. \quad (12)$$

**Marginal and partial contributions of each factor.** For each factor  $f \in \mathcal{F}$  we construct:

- The *marginal* projector

$$P_f^{\text{marg}} = Z^{(f)} (Z^{(f)\top} Z^{(f)})^+ Z^{(f)\top}, \quad (13)$$

which captures the variance explained by factor  $f$  alone.

- The projector onto all *other* factors,

$$Z_{-f} = [Z^{(g)} : g \in \mathcal{F}, g \neq f], \quad P_{-f} = Z_{-f} (Z_{-f}^\top Z_{-f})^+ Z_{-f}^\top. \quad (14)$$

- The *partial* projector of  $f$  given the others,

$$P_f^{\text{part}} = P_{\text{all}} - P_{-f}, \quad (15)$$

analogous to a partial sum-of-squares in ANCOVA.

We then compute the marginal sum of squares, partial sum of squares, and the corresponding  $R^2$  values,

$$SS_f^{\text{marg}} = \text{tr}(AP_f^{\text{marg}}), \quad R_f^2, \text{marg} = \frac{SS_f^{\text{marg}}}{SS_{\text{total}}}, \quad (16)$$

$$SS_f^{\text{part}} = \text{tr}(AP_f^{\text{part}}), \quad R_f^2, \text{part} = \frac{SS_f^{\text{part}}}{SS_{\text{total}}}. \quad (17)$$

We additionally report the partial eta-squared effect size,

$$\eta_{p,f}^2 = \frac{SS_f^{\text{part}}}{SS_f^{\text{part}} + SS_{\text{resid}}}. \quad (18)$$

**Permutation-based significance testing.** To assess whether the partial contribution of factor  $f$  is greater than expected by chance, we perform a label-permutation test. Let  $SS_f^{\text{part}}$  be the observed partial sum of squares for factor  $f$ . For each permutation  $\pi$  of  $\{1, \dots, n\}$ , we:

1. Shuffle the labels of factor  $f$ :  $\tilde{y}_i^{(f)} = y_{\pi(i)}^{(f)}$ .
2. Reconstruct the permuted design  $Z_\pi^{(f)}$  and the full design  $Z_\pi = [Z_\pi^{(f)}, Z_{-f}]$ .
3. Form the permuted projector  $P_{\text{all},\pi}$  and compute

$$SS_{f,\pi}^{\text{part}} = \text{tr}(A(P_{\text{all},\pi} - P_{-f})). \quad (19)$$

Given  $N_{\text{perm}}$  permutations, we define the permutation  $p$ -value as

$$p_f = \frac{1 + \#\{\pi : SS_{f,\pi}^{\text{part}} \geq SS_f^{\text{part}}\}}{1 + N_{\text{perm}}}. \quad (20)$$

**Additive effect vectors in Euclidean space.** When the metric is Euclidean, we can interpret variance partitioning in terms of an explicit linear model on the representation vectors. We write

$$\mathbf{x}_i = \boldsymbol{\mu} + \sum_{f \in \mathcal{F}} \boldsymbol{\beta}_{y_i^{(f)}}^{(f)} + \boldsymbol{\varepsilon}_i, \quad (21)$$

where  $\boldsymbol{\mu} \in \mathbb{R}^d$  is a global intercept, and  $\boldsymbol{\beta}_\ell^{(f)} \in \mathbb{R}^d$  is the effect vector for level  $\ell$  of factor  $f$ . To make the decomposition identifiable, we impose a sum-to-zero constraint per factor,

$$\sum_{\ell=1}^{L_f} \boldsymbol{\beta}_\ell^{(f)} = \mathbf{0}, \quad \forall f \in \mathcal{F}. \quad (22)$$

Let

$$\boldsymbol{\mu} = \frac{1}{n} \sum_{i=1}^n \mathbf{x}_i, \quad X_c = X - \mathbf{1}\boldsymbol{\mu}^\top \quad (23)$$

Table 4. **Example Variance partitioning results for representational factors of T5 contextual word vector.** The model achieves a total explained variance of  $R_{\text{total}}^2 = 0.7486$ .

Feature	Levels	df <sub>eff</sub>	df <sub>res</sub>	SS <sub>tot</sub>	SSR <sub>marg</sub>	R <sub>marg</sub> <sup>2</sup>	SSR <sub>part</sub>	R <sub>part</sub> <sup>2</sup>	$\eta_p^2$	p <sub>perm</sub>
color2shape2	6	5	249	4291.0948	2479.8288	0.5779	1884.9433	0.4393	0.6360	0.0099
spatial_relationship	8	7	249	4291.0948	517.8120	0.1207	517.8120	0.1207	0.3243	0.0099
shape1	3	2	249	4291.0948	809.6197	0.1887	214.7342	0.0500	0.1660	0.0099

be the sample mean and the centered representation matrix. The additive model (21) can be written in matrix form as

$$X_c = ZB + E, \quad (24)$$

where  $B \in \mathbb{R}^{p \times d}$  stacks all effect vectors as rows, and  $E$  collects residuals. We estimate  $B$  by multivariate least squares

$$\hat{B} = \arg \min_B \|X_c - ZB\|_F^2 = (Z^\top Z)^+ Z^\top X_c. \quad (25)$$

The rows of  $\hat{B}$  corresponding to factor  $f$  yield its level-specific effect vectors  $\hat{\beta}_\ell^{(f)}$ . For numerical stability and to enforce the sum-to-zero constraint, we re-center these estimates per factor,

$$\hat{\beta}_\ell^{(f)} \leftarrow \hat{\beta}_\ell^{(f)} - \frac{1}{L_f} \sum_{\ell'=1}^{L_f} \hat{\beta}_{\ell'}^{(f)}. \quad (26)$$

Together, the variance-partitioning statistics  $(R_f^{2,\text{marg}}, R_f^{2,\text{part}}, \eta_{p,f}^2, p_f)$  summarize how much of the representational variance is attributable to each factor, while the effect vectors  $\hat{\beta}_\ell^{(f)}$  describe the direction in representation space associated with each level of each factor.

## **C. Dataset and code availability**

To preserve anonymity, we will publicly release all code, configuration files, and datasets at a permanent URL upon acceptance.

## **D. LLM usage**

The usage of LLM is limited to language polishing and grammar, and literature search. We asked an LLM to suggest surface-level rewrites to improve clarity, grammar, and style for author-written passages. Edits were limited to phrasing and organization at the sentence/paragraph level. We also used an LLM to source papers, and produce brief literature summaries for writing references.